Atmospheric Research 198 (2017) 56–80

Contents lists available at ScienceDirect

Atmospheric Research

journal homepage: www.elsevier.com/locate/atmosres

Variability modes of precipitation along a Central Mediterranean area and their relations with ENSO, NAO, and other climatic patterns

Anastasios Kalimeris[a,*], Ezio Ranieri[b], Dimitra Founda[c], Caroline Norrant[d]

[a] Department of Environmental Technologists, Technological Educational Institute of Ionian Islands, 29100 Zakynthos, Greece
[b] Polytechnic University of Bari, Dicatech, 70125 Bari, Italy
[c] Institute for Environmental Research and Sustainable Development, National Observatory of Athens, Palea Penteli 15236, Athens, Greece
[d] University of Lille, Univ. Littoral Côte d'Opale, EA 4477 – TVES – Territoire Villes Environnement and Société, F-59000 Lille, France

ARTICLE INFO

Keywords:
Central Mediterranean
Precipitation variability
Singular Spectrum Analysis
Wavelet analysis
Synchronization
Climatic variability patterns

ABSTRACT

This study analyses a century-long set of precipitation time series in the Central Mediterranean (encompassing the Greek Ionian and the Italian Puglia regions) and investigates the statistically significant modes of the interannual precipitation variability using efficient methods of spectral decomposition. The statistical relations and the possible physical couplings between the detected modes and the global or hemispheric patterns of climatic variability (the El Niño Southern Oscillation or ENSO, the North Atlantic Oscillation or NAO, the East Atlantic or EA, the Scandinavian or SCAND, and others) were examined in the time-frequency domain and low-order synchronization events were sought.

Significant modes of precipitation variability were detected in the Taranto Gulf and the southern part of the Greek Ionian region at the *sub-decadal* scales (mostly driven by the SCAND pattern) and particularly at the *decadal* and *quasi-decadal* scales, where strong relations found with the ENSO activity (under complex implications of EA and NAO) prior to the 1930s or after the early-1970s. The precipitation variations in the Adriatic stations of Puglia are dominated by significant *bi-decadal* modes which found to be coherent with the ENSO activity and also weakly related with the Atlantic Ocean sea surface temperature intrinsic variability. Additionally, important discontinuities characterize the evolution of precipitation in certain stations of the Taranto Gulf and the Greek Ionian region during the early-1960s and particularly during the early-1970s, followed by significant reductions in the mean annual precipitation. These discontinuities seem to be associated with regional effects of NAO and SCAND, probably combined with the impact of the 1970s climatic shift in the Pacific and the ENSO variability.

1. Introduction

Precipitation is a fundamental parameter in the research of climate dynamics whose extreme spatial variability often enforces its study on a regional and/or sub-regional scale, as have been also suggested by the Intergovernmental Panel on Climate Change for regions located in transitional climate areas (Solomon et al., 2007; Trenberth et al., 2007). The Mediterranean basin consists of an area, whose climate conditions are principally controlled by the descending branch of the Hadley circulation (during the summer and early autumn) and the Westerlies zonal flow during the winter season, both of them being major constituents of the general circulation (e.g., Bolle, 2003). The alternation between these fundamental flow systems couples the Mediterranean precipitation with anomalous pressure distribution patterns of the North Hemisphere, mainly with the North Atlantic Oscillation or NAO (Hurrell et al., 2003; Marshall et al., 2001; Wanner et al., 2001; Polonskii et al., 2004), the East Atlantic or EA (Wallace and Gutzler, 1981; Barnston and Livezey, 1987), the Scandinavian or SCAND (Bueh and Nakamura, 2007), the East Atlantic - West Russian or EA-WR (Ionita, 2014), the Indian Monsoon, and probably with even more distant patterns of global-scale climatic fluctuations, such as the El Niño Southern Oscillation or ENSO (e.g., Allan, 2000; Brönnimann, 2007). The Mediterranean cyclogenesis, which is influenced by NAO, SCAND, and the EA-WR variations (Nissen et al., 2010) along with the sea-atmosphere mass and heat flows, are two extra factors that induce further variability in the regional precipitation.

An anomalous climatic event that was recently affecting the entire Mediterranean basin is the significant decline of precipitation between

* Corresponding author at: Department of Environmental Technologists, Technological Educational Institute of Ionian Islands, Minotou-Giannopoulou Str.1, GR 29100 Zakynthos, Greece.
E-mail address: taskal@teiion.gr (A. Kalimeris).

http://dx.doi.org/10.1016/j.atmosres.2017.07.031
Received 14 March 2017; Received in revised form 9 July 2017; Accepted 31 July 2017
Available online 03 August 2017

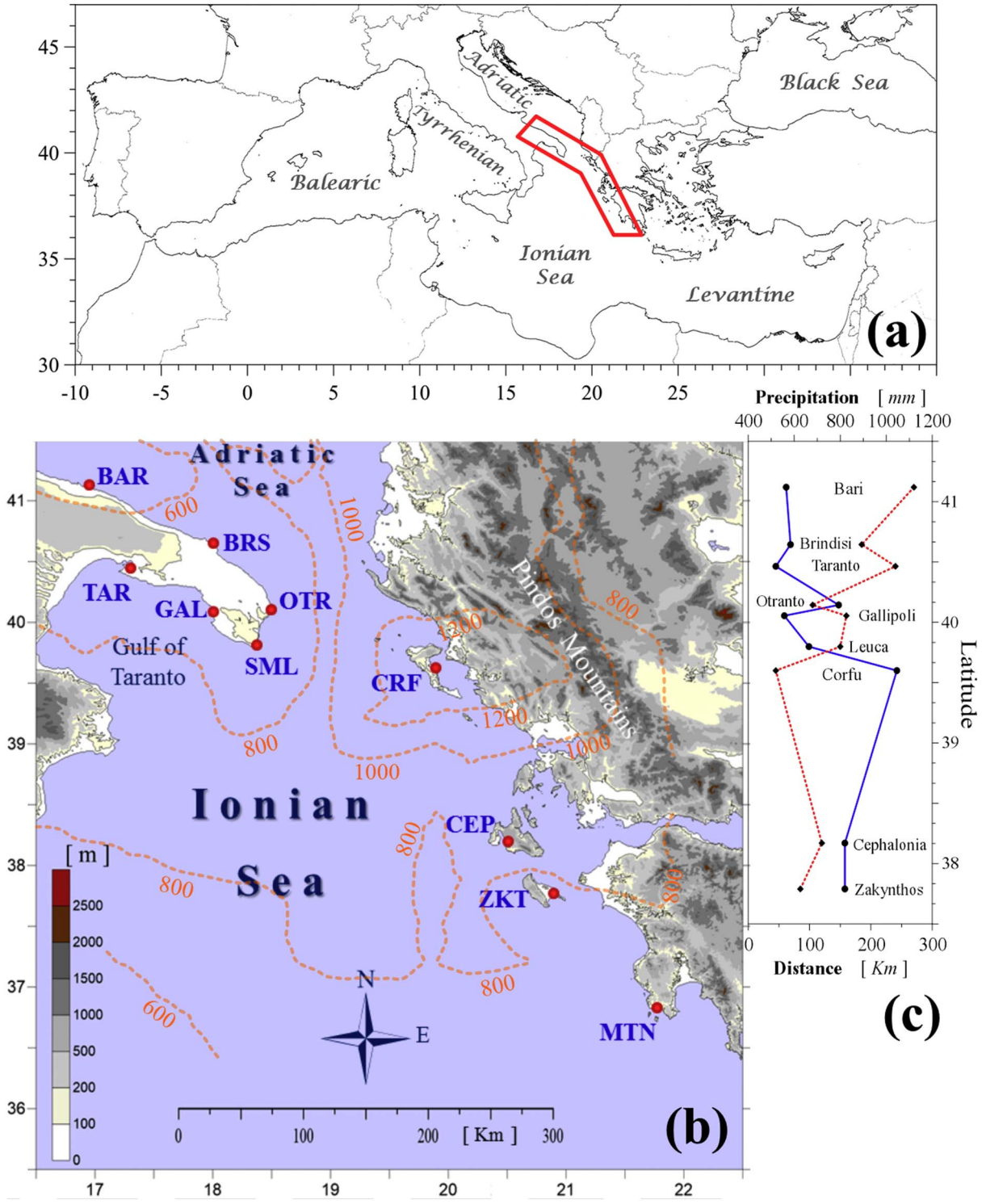

Fig. 1. (a): The location of the studied area in the Mediterranean basin (red polygon).
(b): Geophysical map of the studied area. The position of the ground stations used in this study is indicated by the red dots. The meaning of the acronyms is: Bari (BAR), Brindisi (BRS), Taranto (TAR), Otranto (OTR), Gallipoli (GAL), Santa Maria di Leuca (SML), Corfu (CRF), Cephalonia (CEP), Zakynthos (ZKT), Methoni (MTN). The *annual* precipitation height field curves (in mm) implied by the TRMM over the period 1998–2012, are shown by the orange dashed lines.
(c): Variation of the mean annual precipitation height (over the period 1921–2010) in respect to the latitudinal position of the indicated stations (blue line, scale at the top). The corresponding distance of each rain gauge from the main orography (height ≥ 1 km) of the Balkans coastline is also shown by the red line (scale at the bottom). (For interpretation of the references to colour in this figure legend, the reader is referred to the web version of this article.)

the early 1970s and 2000. This event is caused by a persisting NAO positive phase (initiated at an epoch where protracted El Niño events and strong inter-decadal activity developed in ENSO) under the enhancing effects of SCAND and EA-WR (e.g., Krichak et al., 2002; Krichak and Alpert, 2005). Then, dryness became more evident in parts of the Central and Eastern Mediterranean, particularly in the Italy–Greece region (Norrant and Douguédroit, 2005). This area, which is actually comprised by the Ionian Sea (Fig.1a), is one of the least-studied

and sub-sampled parts of the Mediterranean basin. Additionally, the spatiotemporal precipitation variability over the Ionian Sea has an increased oceanographic interest due to its role in the dynamics of the Mediterranean Sea circulation and its implications in important oceanographic processes like the Eastern Mediterranean Transient or EMT, that occurred from the late 1980s to about 2000 (Malanotte-Rizzoli et al., 1997; Borzelli et al., 2009; Gačić et al., 2011, 2012). Earlier studies have shown that negative secular trends of precipitation prevail in the Italian regions of Calabria, Sicily, and the Greek Ionian region, and mixed weak trends in Puglia (Federico et al., 2010; Buttafuoco et al., 2011; Caloiero et al., 2011; Kalimeris et al., 2012; Coscarelli and Caloiero, 2012; Arnone et al., 2013). Furthermore, many climate model simulations in regional (Lionello and Giorgi, 2007; Gualdi et al., 2013) and sub-regional scales (e.g., Kalimeris et al., 2012) anticipate mild (0% to −10%) precipitation deficits in the southern Italy and Puglia until the end of the current century, but greater losses (−5% to −20%) in the Greek Ionian region.

In this framework, the significant modes of precipitation variability are searched for here, along two marine areas, the Italian region of Puglia and the Greek Ionian Islands, which form a cohesive *marine-islanding environment* stretching meridionally by almost 650 km in the Central Mediterranean (Fig.1a). The availability of historical -century long- precipitation records from local ground-based stations offers an opportunity to set-up a detailed local "meridional tomography" of the Central Mediterranean climatic variability. Hence, the current study aims to: (a) detect the significant modes of precipitation in the studied area and examine their time evolution, (b) explore the statistical relations and the underlying physical couplings of the detected modes with the main patterns of climatic variability in different time-scales, and (c) assess the response of the regional precipitation to significant global-scale climatic fluctuations during the last century. For these purposes, the general characteristics of the precipitation variability and of the underlying climate dynamics along the studied area, are briefly reviewed in Section 2. The adopted *monthly* precipitation data sets and the applied analysis methods are introduced in Section 3. Results are presented in Section 4, while the implied physical picture of the precipitation climatic dynamics in the studied area during the last century is discussed in Section 5.

2. Description of the study area

Puglia (or Apulia) is an elongated area that invades into the Ionian Sea by the nearly flat peninsula of *Salento* and shapes the Gulf of Taranto in its western side, while it sets the southern boundaries of the Adriatic Sea at the Strait of Otranto (Fig.1b). At the southern extension of Puglia, the mountainous Ionian Islands are deployed parallel to the western Greek mainland at a small distance from Pindos Mountain range.

Both Puglia and the Greek Ionian region are freely exposed to strong *sirocco*–type southern winds which are imposed by the frequent passage of Mediterranean and Northern Africa cyclones (Meteorological Office, 1962; Homar et al., 2007; Bartholy et al., 2009). Due to the relatively high sea surface temperature (SST) the Ionian region becomes a major contributor of humidity at a basin-wide scale (Romanou et al., 2010; Schicker et al., 2010; Zveryaev and Hannachi, 2011). Because sirocco is a strong far-fetched lowest troposphere flow system, it efficiently streams the moisture, the sensible, and the latent heat towards the steep coastal orography of western Balkans and Greece, where the airflow experiences horizontal convergence and uplift due to counter-balanced divergence. Thus, a *wind convergence zone* often develops along the *western Balkans* and forced convection, able to evolve in thunderstorm cells and heavy precipitation, prevails. The relation between cyclonic activity, sirocco winds, and local heavy precipitation events has been long established and studied in details along the Adriatic and western Balkans (e.g., Pasarić et al., 2007; De Luis et al., 2013; Ivančan-Picek et al., 2014), the southern Italy (Horvath et al., 2008; Miglietta and Regano, 2008; Moscatello et al., 2008; Federico et al., 2008; Mastrangelo et al., 2011), and recently for the north-western Greece (Sindosi et al., 2015).

The studied area is also affected by the outbreaks of northern *Bora* as it is channeled through the Adriatic, and by the northeastern *Gregale*. The Italian orography of Basilicata and Calabria regions further causes a variety of intense mesoscale dynamic phenomena and heavy precipitation events (studied in details by Mastrangelo et al., 2011; Federico et al., 2008) which can seriously affect the Gulf of Taranto, Salento, and the Central Ionian Sea. Another mesoscale process that influences the precipitation along Puglia under weak synoptic conditions is the development of a double see-breeze system originating from the opposite coasts of Salento. This system drives in the formation of a local convergence zone along the peninsula, often accompanied by convective precipitation (Mangia et al., 2004; Comin et al., 2015).

An overview of the regional mean *annual* precipitation height field, as implied by the Tropical Rainfall Measuring Mission or TRMM (Huffman et al., 2007) for the period 1998–2012, is shown in Fig.1b (Kolios and Kalimeris, 2016). The impact of the western Balkans convergence zone in the spatial precipitation distribution becomes apparent in Fig.1b,c by the strong anti-symmetric relation between the recorded annual precipitation height and the distance of each station from the significant orographic barriers of the Balkans coastline.

3. Material and methods

3.1. Data, missing values, and homogenization

Monthly precipitation data from six coastal stations in Puglia (as indicated in Fig.1b) for the period 1921–2010 were adopted in this study by the *Italian Hydrographic Office*. A second data-set for the Greek Ionian stations, covering the period 1893–2010, was provided by the *National Observatory of Athens* (NOA) and by the *Hellenic National Meteorological Service* (HNMS), supplemented for the period 1956–2010 by the Ionian coastal station of *Methoni* at the southern tip of Peloponnesus. A concise review of the available precipitation data along with missing values indices are given in Table 1.

After data quality control through *CLIMATOL* (Guijarro, 2011), missing values estimation and *relative homogenization* of the observed monthly precipitation series was performed through the *HOMER* (Mestre et al., 2013) and *ACMANT*$_2$ (Domonkos, 2015) algorithms, as described in Appendix A. The corrected series implied by *HOMER* and *ACMANT*$_2$ were found to be very similar and only in a few cases the *HOMER* series declined from the original observations slightly more than the *ACMANT*$_2$ series (in this sense, the *HOMER* series might be considered as a reliable upper limit of the implied corrections). For example, the original and the corrected precipitation series for two representative stations of the studied area are illustrated in Fig. A1 (Appendix A). Taking also into account the study of Venema et al. (2012), the *HOMER* series were adopted throughout the subsequent analysis. Descriptive statistics and linear trends in the original and the corrected precipitation series for each station are also given in Table 1. Due to the well-defined precipitation minimum in July along all stations of the studied area, the annual heights are referred here to a typical Mediterranean *hydrological year* (in the sense of a rainfall year season) considered as the interval from July 1st of the *i*-year, to June 30th of the year $i + 1$.

Regarding the state of the aforementioned patterns of climatic variability, two classic indices were adopted for ENSO, the Niño-3.4 (that express the SST anomalies averaged over the equatorial Pacific area 5°N–5°S and 170°–120°W) and the Southern Oscillation Index or SOI (that expresses the differences of the standardized pressure anomalies between Tahiti and Darwin in the tropical Pacific). Monthly Niño-3.4 values were obtained from the Climate Prediction Center of the National Oceanic and Atmospheric Administration (CPC/NOAA), while SOI values were obtained from the Working Group on Surface

Table 1
The observational period covered in each station (1st row) along with the number of the available *annual* (N_a) and *monthly* (N_m) values (rows 2–3). The percentage of missing data in each *monthly* series is given by MD_m (row 4) and the maximum number of *consecutive years* with at least one missing month is given by MD_{ac} (row 5). The finally available *annual* and *monthly* observations n_A and n_M after missing data filling are listed in rows 6–7. The mean annual precipitation values $\overline{H}_H$ over the observational period and over the common period 1921–2010 ($\overline{H}_C$) are listed in rows 8–9 (in mm). Finally, the linear trends (in mm/year) in the original ($\overset{?}{H}_o$) and the corrected ($\overset{?}{H}_H$) series are given over the observational period (rows 10–11) and over the common observational period 1921–2010 ($\overset{?}{H}_C$) in the last row (whenever applicable).

		Bari	Brindisi	Taranto	Otranto	Gallipoli	Leuca	Corfu	Cephalonia	Zakynthos	Methoni
Observations period		1938–2010	1921–2010	1921–2010	1921–2010	1921–2010	1921–2010	1887–2010	1893–2010	1893–2010	1956–2010
Initial data	N_a	67	88	88	87	89	85	105	95	95	54
	N_m	826	1062	1062	1062	1078	1031	1452	1247	1278	647
	MD_m	5.7%	1.7%	1.7%	1.7%	0.2%	4.5%	2.5%	8.9%	9.0%	0.01%
	MD_{ac}	5	1	1	1	2	2	6	11	10	1
Final data	n_A	73	90	90	90	90	90	124	118	118	55
	n_M	876	1080	1080	1080	1080	1080	1488	1416	1416	660
Mean values	$\overline{H}_H$	565.0	584.5	519.8	793.0	557.4	663.5	1066.7	839.7	855.3	689.1
	$\overline{H}_C$		584.5	519.8	793.0	557.4	663.5	1045.6	823.6	820.9	
Linear trends	$\overset{?}{H}_o$	-0.13	+ 0.86	+ 1.01	-0.65	+ 0.33	+ 0.32	**-1.94**	-0.47	**-2.69**	-1.28
	$\overset{?}{H}_H$	-0.13	+ 0.86	-0.18	-0.65	+ 0.33	+ 0.32	-0.60	-0.42	**-1.10**	-1.28
	$\overset{?}{H}_C$		+ 0.86	-0.18	-0.65	+ 0.33	+ 0.32	+ 0.36	+ 0.32	-0.22	

Bold underlined values indicate statistically significant trends at the 0.05 level.

Pressure/ Global Climate Observing System or WG-SP/GCOS. The adopted NAO, EA, EA-WR, and SCAND indices were based on the leading Rotated Principal Component Analysis (RPCA) Empirical Orthogonal Functions (EOFs) of the monthly standardized 500 hPa height anomalies over the 20°–90°N region, and they were obtained for the period after 1950 from the CPC/NOAA and the National Centers for Environmental Prediction / National Center for Atmospheric Research (NCEP/NCAR) reanalysis climate data assimilation system. Additionally, the classic ground-station NAO index of Hurrell and National Center for Atmospheric Research Staff (2016) was adopted (hereafter referred as the NAO HSt index). Finally, the monthly average values of the equatorial stratospheric (30 hPa) zonal wind obtained from NCEP/NCAR, and adopted as an exploratory index for the quasi-biennial oscillation or QBO.

3.2. Methods of climatic signal analysis

The search of statistically significant modes in the precipitation variability of the studied area is performed here through a multi-spectral decomposition procedure which is primarily based on the efficient data-adaptive *Singular Spectrum Analysis* or SSA (Allen and Smith, 1996; Elsner and Tsonis, 1996; Ghil et al., 2002, and references therein). Each monthly series is decomposed by SSA into *non-linear trends*, *oscillatory components*, and *stochastic variations*. The oscillatory components are efficiently detected in the periodicities range or time-scales band ($M/5$, M) where M is the embedded dimension or window width (Yiou et al., 1994). An optimal choice of M, reflecting a compromise between high statistical confidence (low M values) and high spectral resolution (high M values), has to be made through a set of preliminary computations. Then, the frequency f of oscillatory terms whose variability is characterized by a timescale s longer than M, may be not well specified (such terms are then referred as "*slow*" components). To extend the detectability limit towards longer time-scales, a window length corresponding to 20–25 years was adopted here, depending on the exact length n of each series. The *temporal* empirical orthogonal functions or T-EOFs (eigenvectors of the observed precipitation series $M \times M$ lag-covariance matrix C_X) and the associated temporal principal components or T-PCs (the projections of the time series onto the T-EOFs) were consequently computed for the annual, the monthly, and the *extended winter* (December to March, or DJFM) versions of each series.

To obtain a useful preliminary view of the main features in the power spectral density function S(f), the *Blackmann-Tukey* (BT) or windowed correlogram (Blackman and Tukey, 1958), the *Maximum Entropy Method* or MEM (Burg, 1967; van den Boss, 1971), and the *revised Multi-Taper Method* or MTM (Mann and Lees, 1996) were sequentially applied prior SSA. This procedure helps in reducing the by-chance detection of significant components through SSA and further in estimating possible spectral aliasing effects. Subsequently, wavelet analysis was applied by means of the *Continuous Wavelet Transform* (Foufoula-Georgiou and Kumar, 1995; Grinsted et al., 2004; Torrence and Compo, 1998) in order to examine the evolution of the significant variability modes of precipitation in the time-frequency domain, particularly of those which are detected by SSA. The Morlet function (with a wavenumber $\omega_0 = 6$) was selected as a mother wavelet since it represents a functional basis well localized in both time and frequency that has been proved to perform well in the analysis of a wide variety of geophysical time series (Foufoula-Georgiou and Kumar, 1995; Grinsted et al., 2004). As explained in Appendix B, the time scale s corresponding to the adopted Morlet wavelet almost coincides with the Fourier wavelength (or period), hence, it is used here as an equivalent of the Fourier wavelength.

Statistical significance of the spectral components was tested against the null-hypothesis $\mathscr{H}_0$: "*the observed series is nothing more than red noise realizations*" according to the procedure described by Allen and Smith (1996) for SSA, by Mann and Lees (1996) for the revised MTM, and by Torrence and Compo (1998), and Grinsted et al. (2004) for wavelet. Hereafter, the term "*significant*" will be used to signify *statistical significance at the* 0.05 *confidence level*. Finally, reconstruction of the significant components in the time domain was computed according to the procedure described by Ghil et al. (2002). The *reconstructed components* (RCs) reproduce the *amplitude evolution* of each term and capture its *phase* variations at a frequency f or scale s. In order to dump the possible interferences of the annual precipitation cycle with other time-scales, the *centralized* monthly precipitation series were used throughout the subsequent analysis.

4. Results

As it is seen in Table 1 (see the "mean values" section) the precipitation distribution in the Greek Ionian region reflects the typical southwards decrease of the mid-latitudes along with the weakening effects of the western Balkans wind convergence zone in this direction.

On the other hand, a reversed precipitation gradient is observed along the peninsula of Salento (consistent with the distribution found through the TRMM data-sets in Fig.1b) which proves to be a time persistent and statistically significant characteristic ($p < 0.01$) through a Mann-Whitney test. Additionally, it is worth noting that a *reduction* of the mean annual precipitation value followed after each significant discontinuity event, particularly those detected at the 1960s and at the 1970s (Appendix A).

Regarding the *linear–secular-trends* (Table 1) it is seen that in reference to the common observational period 1921–2010, *mixed non-significant trends* prevail in Puglia (ranging from + 0.86 to − 0.65 mm/year) and in the Greek Ionian region (+ 0.36 to − 0.22 mm/year). However, *strong negative trends prevail in the Greek Ionian stations* (particularly in *Corfu* and *Zakynthos*) when the entire observational period 1893–2010 is considered (see also Fig.A1).

In order to resolve the main spatial patterns of precipitation variability in the studied area, the Varimax orthogonal rotation method (Kaiser, 1958) was applied in a subset of Principal Component Analysis EOFs of the matrix $\mathscr{R}$, over the common observations period 1921–2010. The eigenvalues spectrum λ_k [with k ranging from 1 to 10 at a unit step, hereafter annotated as $k = 1(1)10$] of the corresponding un-rotated EOFs indicate that only the first two eigenvalues corresponding to EOF1 and EOF2 are non-degenerate (embedded graph in Fig.2). The spatial distribution of the loadings (which represent the correlation of each rotated EOF with the variations of the annual precipitation in each station) is illustrated in Fig.2. As can be seen there, the rotated EOF1 is associated with the precipitation variability of Puglia stations, while EOF2 reflects the variability of the southern Greek Ionian region. These rotated EOFs jointly account for 65% of the variance in the correlation matrix $\mathscr{R}$. The corresponding rotated Principal Components (or RPCs) collectively represent the monthly precipitation series in Puglia (RPC1) and the southern Greek Ionian region (RPC2).

4.1. Precipitation variability modes

The SSA, MTM, and wavelet spectra of the monthly precipitation series are illustrated in Fig.3 (for definitiveness the BT and MEM spectra are omitted). The prominent spectral components resulted from SSA, MTM, MEM, and BT methods are also listed in Table 2, in six time-scale bands: the *biannual* (1–3 years), the *short* (3–5 years), the *sub-decadal* (5–8 years), the *decadal* (8–16 years), the *bi-decadal* (16–30 years), and the *multidecadal* (considered here as those with $s \geq 30$ years). In this framework, the significant modes of precipitation variability that were found along the studied area can be organized as follows:

i) *Sub-decadal modes* having the form of oscillatory variations are widely met at the *quasi-biennial* or QB band (2–3 years) in all stations, particularly in southern Puglia where they account for a remarkable 37–40% of the total precipitation variance in *Leuca* and *Gallipoli* (Figs.3e,f and 4a). Oscillatory modes were also found at the short scales (3–5 years) in many stations, particularly in *Cephalonia* and *Taranto* where they account for 15–19% of the total variance (Figs.3c,h and 4b). Finally, significant sub-decadal modes were found at 7–8 years, mainly in the southern Greek Ionian region accounting for 12.5% of the total variance in *Zakynthos* (and 23% in

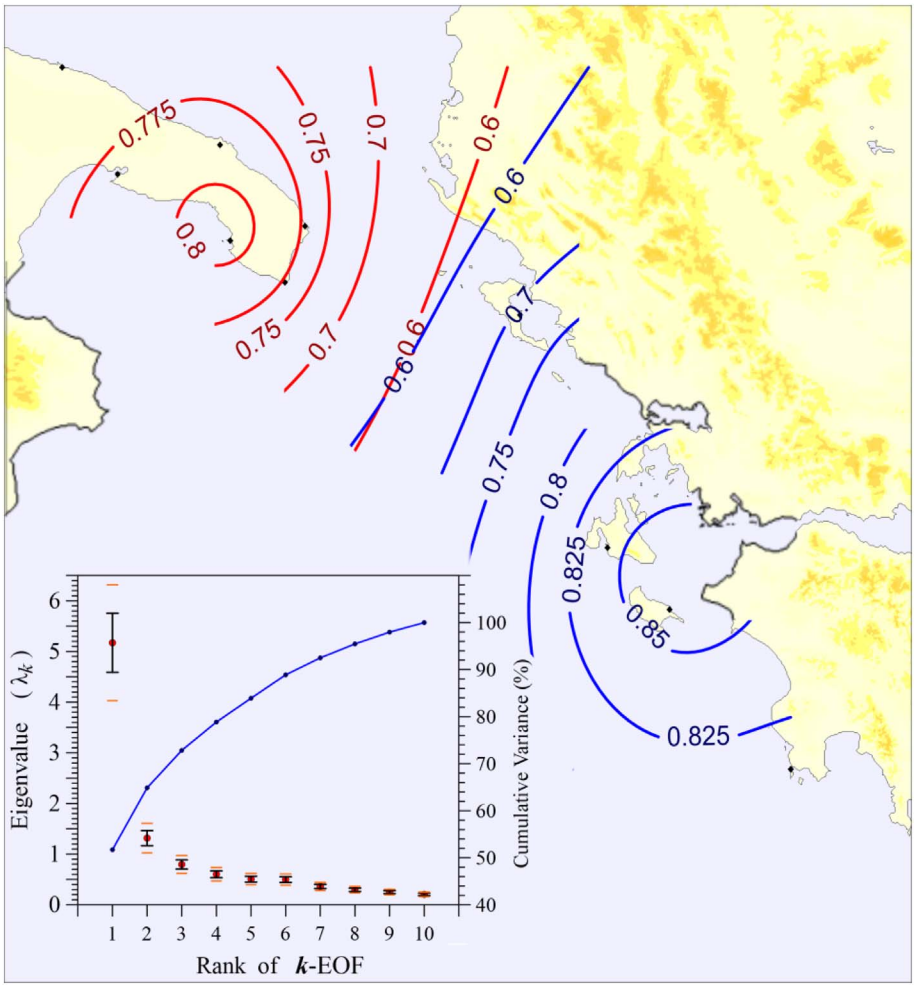

Fig. 2. Normalized loadings of the precipitation RPCA factors, with the rotated EOF1 displayed by the red curves and EOF2 by the blue curves. The eigenvalue spectrum of the corrected precipitation correlation matrix $\mathscr{R}$ is shown in the embedded graph (lower left) along with the error bars and the 95% confidence interval limits (orange lines). The accounted cumulative variance is depicted by the blue curve in this graph (scale on the right). (For interpretation of the references to colour in this figure legend, the reader is referred to the web version of this article.)

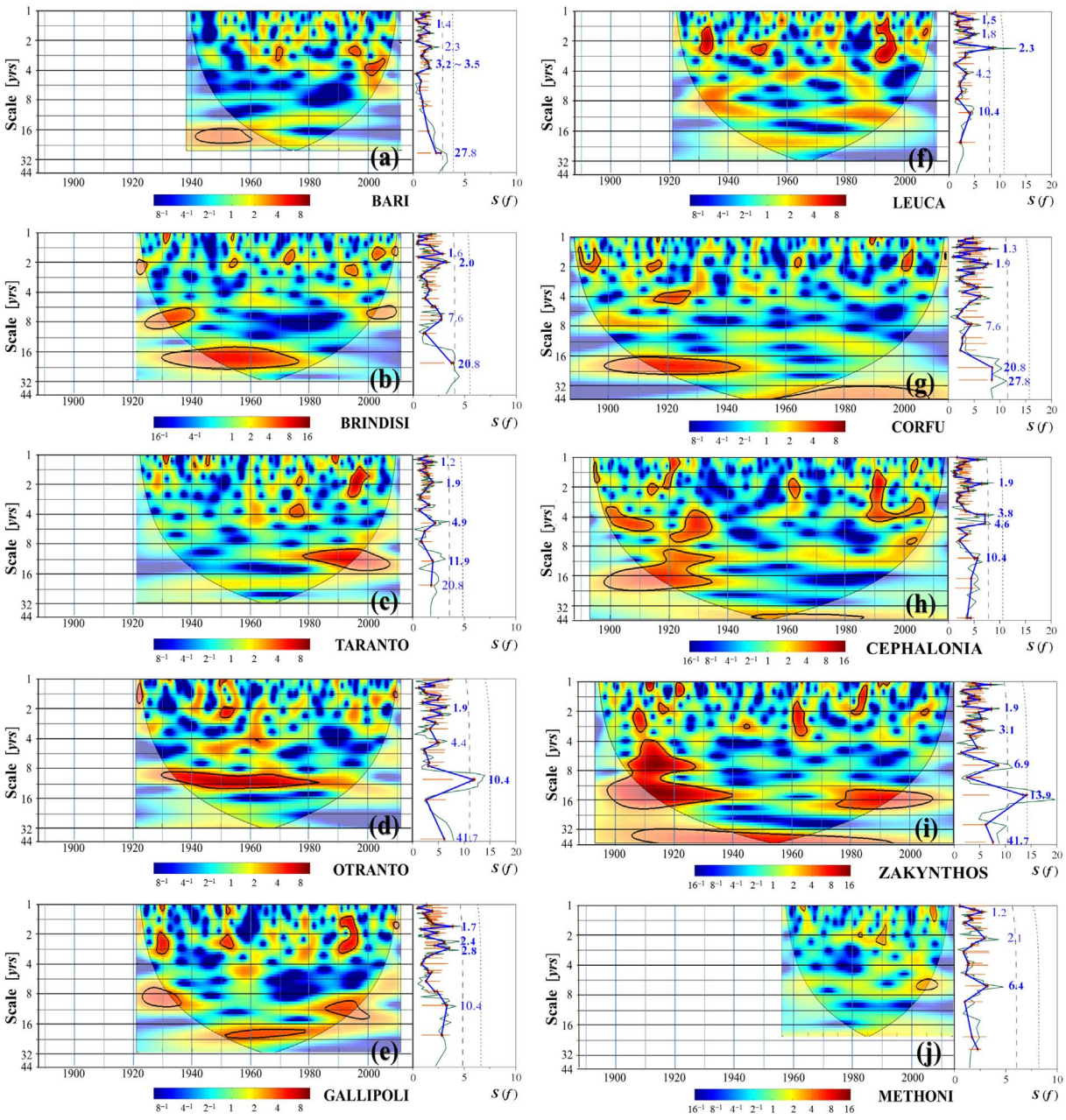

Fig. 3. Wavelet power spectra of the centralized monthly precipitation series (dates are shown at the horizontal axis). The power scale at the lower part of each panel is referred to the variance units (σ^2) of the corresponding series, while the statistically significant (at the 0.05 level) regions are bordered by the bolded black lines. The SSA (blue lines) and MTM (green lines) spectra are additionally illustrated at the right part of each panel with the S(f) power density function units referred in 10^3 mm^2. The small orange bars in the SSA spectra indicate the 2.5% and 97.5% percentiles of the Monte Carlo red-noise simulations, while the long- and the short-dashed lines respectively signify the 90% and 95% confidence levels of the AR(1) red noise background in the MTM spectra. The central periodicities values (in years) of the prominent SSA components are also indicated. As we are interested for the interannual precipitation variability, the high-frequency spectral tails (f ≥ 0.083 months^{-1} or scales $s \leq 12$ months) have been clipped. Notice the different power scales among panels. (For interpretation of the references to colour in this figure legend, the reader is referred to the web version of this article.)

Methoni where data are available only after 1956). A similar mode dominates the winter precipitation variations in *Corfu* at 7.6 years, while in Brindisi this mode is sensed as marginally significant by SSA.

ii) *Decadal and quasi-decadal modes* are mostly detected in the southern Puglia and Greek Ionian region at the 10–16 years band. They are particularly manifested by exceptionally strong decadal oscillations in *Otranto* (centered at 10.4 years) and by quasi-decadal variations in *Zakynthos* (centered at about 14 years), respectively accounting for 25% and 20% of the total local variance (Figs.3d,i and 4c). Similar modes are also found in *Taranto* at 11.9 years (Figs.3e, 4c), as well as in *Gallipoli*, *Leuca*, and *Cephalonia*, accounting for 10–14% of the total precipitation variance (Table 2). Unlike the Otranto case, these modes are particularly active either *before* the 1940s *and/or after* the 1970s (Fig.3), both being periods of exceptionally strong ENSO-related climatic fluctuations in a global-scale (e.g., Wang, 1995; Allan, 2000; Rimbu et al., 2003)

iii) *Bi-decadal modes* (centered at 21 and 28 years) were detected in *Bari*, *Brindisi*, *Taranto*, and *Corfu*, where they account for 18–19% of the total variance (Figs.3 and 4d).

iv) *Multidecadal* modes in form of long irregular fluctuations were detected in *Otranto*, *Brindisi*, *Corfu*, and *Zakynthos*, actually identified as non-linear trends (or NLT) by SSA with characteristic scales of the order of 40–60 years (i.e., at the upper detectability limit of the

Table 2
The central periodicities of the prominent spectral components detected by SSA, MTM, MEM, and BT (bolded underlined values indicate statistical significance at the 0.05 level). The number of significant modes found in each station is referred in the first row along with the totally explained variance. The partially explained variance by significant modes in each band is also shown in the yellow shaded rows (values in parenthesis are referred to the explained variance by prominent but not-significant modes).

Time-Scale Band [*yrs*]	Method	STATIONS									
		Bari 2 modes 38 %	**Brindisi** 2 modes 44 %	**Taranto** 3 modes 51 %	**Otranto** 2 modes 42 %	**Gallipoli** 1 mode 37 %	**Leuca** 2 modes 62 %	**Corfu** 2 modes 40 %	**Cephalonia** 2 modes 35 %	**Zakynthos** 3 modes 58 %	**Methoni** 1 mode 23 %
1 – 3 (biannual)	SSA	**1.4**, 2.3	**1.6** , **2.0**	**1.2** , **1.9**	**1.9**	**1.7** , **2.4** , **2.8**	**1.5** , **1.8** , **2.3**	**1.3** , **1.7** , **1.9**	**1.9**	**1.5** , **1.9**	1.2 , 2.1
	MTM	1.4 , 1.7 , 2.3	1.6 , 2.0	1.2 , 1.9	1.9 , 2.3	1.7 , 2.4 , 2.9	1.5 , 1.8 , **2.3**	1.3 , 1.7 , 1.9	**1.8**	1.5 , 1.9	1.2 , 2.1
	MEM / BT	1.4 , 1.7 , 2.3	1.6 , 1.9 , 2.0	1.2 , 1.9	1.9 , 2.3	1.6 , 2.4 , 2.8	1.5 , 1.8 , **2.3**	1.3 , 1.7 , 1.9	1.9	1.5 , 1.9	
	Ex. Var.	**4.6%**	**15.4%**	**9.9%**	**6.7%**	**37.1%**	**40.6%**	**21.1%**	**7%**	**10.3%**	(17%)
3 – 5 (short)	SSA	**3.2** , **3.5**		**4.9**	**4.4**		**4.2**		**3.8** , **4.6**	**3.1**	
	MTM	3.2 , 3.9		**4.7**	4.3		4.1		**3.8** , **4.7**	3.1	
	MEM / BT	3.7		4.7	4.5		4.1		3.8 , 4.6	3.1	
	Ex. Var.	**15.7%**		**15.4%**	**10.2%**		**9.8%**		**18.5%**	**8.3%**	
5 – 8 (sub-decadal)	SSA		7.6							**6.9**	**6.4**
	MTM		6.6							**7.4**	6.6
	MEM / BT		7.4 / 7.1							7.1	6.4
	Ex. Var.		(12.8%)							**12.5%**	**23%**
8 – 16 (decadal)	SSA			**11.9**	**10.4**	10.4	**10.4**		**10.4**	**13.9**	
	MTM			11.4	9.5	10.7	9.5		11.4	**15.5**	14.2 / - -
	MEM / BT			10.7 , 11.4	10.7	9.0 , 10.0	10.7		10.4 / 10.7	**13.1** / **14.2**	
	Ex. Var.			**13.5%**	**24.7%**	(14%)	**11.5%**		**10.2%**	**20.2%**	
16 – 30 (bi-decadal)	SSA	**27.8**	**20.8**	**20.8**				**20.8** , **27.8**			
	MTM		**19.0** , **28.4**	19.0		28.4		21.3 , 28.4	21.3	28.4	21.3
	MEM / BT	28.4	17.1 , 24.4	21.3 / - -		28.4		21.3 / 24.4	17.1 / - -		21.3
	Ex. Var.	**19.3%**	**17.7%**	**12.5%**				**14.5%**			
> 30 & NLT (multi-decadal)	SSA		**NLT**		41.7			**NLT**		**41.7** , **NLT**	NLT
	MTM	**34.0**			42.7			57	57	**57**	
	MEM / BT	43	34.1		42.7			42.7	42.7 / - -		
	Ex. Var.		**11%**		(6.4%)			**4.5%**		**6.5%**	(11.1%)

utilized methods). These components account only for a small amount (5–11%) of the total precipitation variance (Figs.3 and 4e).

The local strength of the detected SSA modes can be represented by the normalized *excessive spectral power* $\mathcal{P}_{E,k}$ of the *k*-EOF, which is defined here as:

Hence, in each station $\mathcal{P}_{E,k}$ is a measure of the power surplus ($P_k - P_{k,*}$) of the *k*-EOF above the estimated red-noise threshold ($P_{k,*}$), normalized by the local total variance ΣP. The spatial distribution of $\mathcal{P}_{E,k}$ is depicted according to the different time-scales in Fig.5. The dominance of the QB precipitation modes in the southern Puglia (Fig.5a), the wide-spreading of the decadal and quasi-decadal modes (Fig.5d), and the prevalence of the bi-decadal modes in the Adriatic stations (Fig.5e), are some of the most important features.

4.2. Relations with the principal atmospheric and coupled ocean-atmosphere processes

We explore in this section the statistical relations of the detected precipitation variability modes with the principal atmospheric and coupled ocean-atmosphere processes which are known for their ability to drive or induce climatic fluctuations in the Euro-Mediterranean area. The possible relations with ENSO are first explored in Section 4.2.1, and then, those with the main Northern Hemisphere's mid-latitudes natural atmospheric variability modes (NAO, EA, EA-WR, and SCAND) are searched in Sections 4.2.2 to 4.2.5. Because of the detection of strong QB precipitation modes at 2.3–2.4 years, the possible statistical relations with the QBO are also examined in Section 4.2.6.

In the subsequent analysis each climatic pattern is considered as a chaotic oscillator whose signals (variability effects) propagate through the global circulation and the ocean-atmosphere interactions in very long distances, thus inducing variations in sub-regional climatic systems (like the studied one), which are further supposed to behave as uni-directionally *coupled* oscillators. Among the great diversity of variability modes that may prevail in the coupled system, those associated with *synchronization* (e.g., Rosenblum et al., 1996; Pikovsky et al., 2003) and with *stochastic resonance* processes (e.g., Benzi et al., 1982; Nicolis, 1993) have been studied more extensively in the framework of dynamical systems and climate dynamics. Synchronization events are of specific importance since they can be developed even under weak coupling, provided that a regional climatic system behaves as a self-sustained or an excitable oscillator (Pikovsky et al., 2003; Crucifix, 2012), otherwise linear and non-linear resonance events might also emerge.

In isolated oscillating systems, three distinct synchronization regimes of order *n*:*m* (*n* pulses of the oscillator within *m* cycles of the coupled system) are expected as the degree of coupling increases (Pikovsky et al., 2003; Osipov et al., 2003; Feliks et al., 2010): i) a frequency or *f-type* locking, where phases and amplitudes can remain uncorrelated, ii) a frequency *and* phase locking or *fp-type* synchronization, where amplitudes can remain uncorrelated, and iii) a frequency, phase, *and* amplitude locking or *fpa-type* synchronization (also referred as *generalized synchronization*). In a regional climatic system which is imposed to quasi-periodic forcing in the presence of noise, stochastic resonance can also emerge under favorable conditions (typically, an appropriate combination between the instantaneous driver phase and the noise level). In such processes, abrupt *transitions* of the coupled system between different variability modes can be triggered, and possibly being detected as discontinuities in the corresponding time series (e.g., Alley et al., 2001; Pikovsky et al., 2003; Tsonis et al., 2007; Wang et al., 2009). However, in the actual geophysical world where an oscillating system is only part of a continuous oscillatory medium and the coupling strength is variable, the induced variability associated with synchronization or resonance processes might be much more

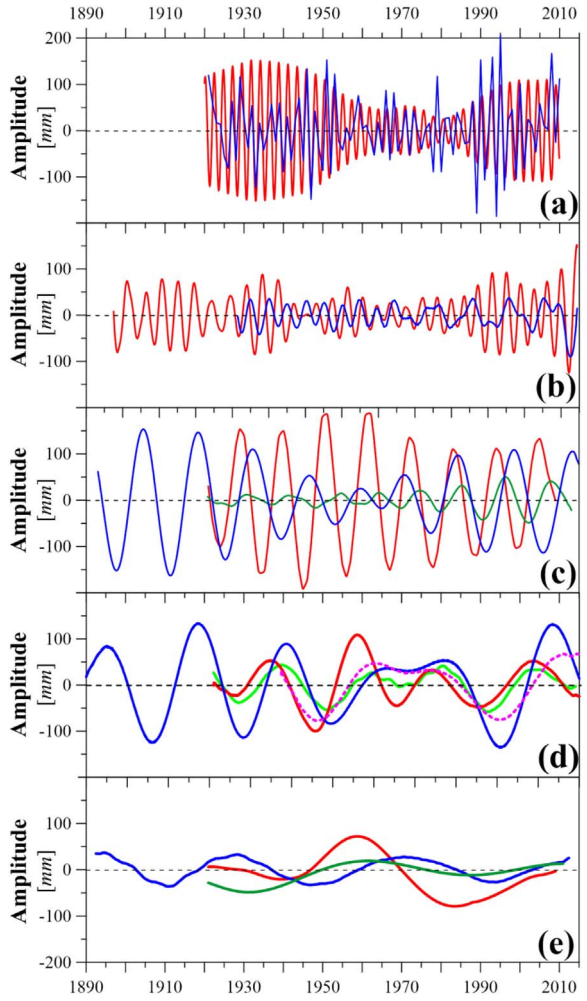

Fig. 4. (a): The SSA components at 2.3 years in Leuca (red curve) and at 2.4–2.8 years in Gallipoli (blue curve).
(b): The combined effect of the short scale SSA components at 3.8 and 4.6 years in Cephalonia (red curve) and at 4.9 years in Taranto (blue curve).
(c): The SSA precipitation mode at 10.4 years in Otranto (red curve), at 11.9 years in Taranto (green curve), and at 13.9 years in Zakynthos (blue curve).
(d): The bi-decadal SSA modes at 21 years in Brindisi (red curve) and Taranto (green curve), along with the 28 years mode in Bari (magenta dashed curve). The combined effect of the 21 and 28 years modes in Corfu are depicted by the blue curve.
(e): The multidecadal SSA modes at 42 years in Otranto (red curve), in Zakynthos (blue curve), and the non-linear trend in Brindisi (green curve). (For interpretation of the references to colour in this figure legend, the reader is referred to the web version of this article.)

complicated and hardly resolved.

Quantification of the relationship between two time series $x(t_j)$, $y(t_j)$, $j = 1(1)n$, corresponding the first to the driver and the second to a coupled oscillator, entangles estimations of their amplitudes $\alpha_x(t_j)$, $\alpha_y(t_j)$, phases $\varphi_x(t_j)$, $\varphi_y(t_j)$, and frequencies $f_x(t_j)$, $f_y(t_j)$. Then, the evolution of these relations in the time-frequency or the *time-scale* domain can be estimated as described in Appendix B by four quantities: (i) the Cross-Wavelet Transform $W_{t_j}^{xy}(s)$ as a localized measure of the common power between $x(t_j)$ and $y(t_j)$ at the time t_j and scale s, indirectly reflecting the covariance of their amplitudes α_x, α_y, (ii) the wavelet coherence $R_{t_j}^2(s)$ as a measure of their correlation in the time-scale domain, (iii) the trace in time of the maximum power scales $s_{x,k}(t_j)$, $s_{y,l}(t_j)$ of two modes k, l (in the x, y series, respectively), as a measure of their corresponding frequencies $f_{x,k}(t_j)$, $f_{y,l}(t_j)$, and (iv) the cyclic relative phase $\delta\varphi_c(t_j)$, as a measure of the phase difference between the modes k, l, computed here in reference to the evolving scale $s_m(t_j)$ of the driver oscillator. Although these quantities will be subsequently used as indicators of possible 1:1 order synchronization events, *a complete synchronization analysis is beyond the scope of this exploratory study*. Nonetheless, the Pearson linear correlation coefficient r_p values between the RPC1,2 series with the adopted climatic indices are further given in Table 3, where the Atlantic Multidecadal Oscillation (or AMO) SST index has been also included for the reasons discussed later in Section 5.

4.2.1. Relations with ENSO

The ENSO effects in the Mediterranean area are a field of increasing interest as its signatures in the climatic variability of the Euro-Mediterranean sector have been reported by many researchers (e.g., Fraedrich and Muller, 1992; Mariotti et al., 2002; Alpert et al., 2006; Brönnimann et al., 2007) often in association with the state of regional climatic anomaly patterns (e.g., Rodó et al., 1997; Huang et al., 1998; Hoerling and Kumar, 2000; Mokhov and Smirnov, 2006; Zanchettin et al., 2008) or with the processes entangled in the physical coupling with the greater Euro-Atlantic area (Pozo-Vázquez et al., 2001; Lau and Nath, 2001; Ineson and Scaife, 2009; OrtizBevia et al., 2010).

4.2.1.1. ENSO related effects at the sub-decadal scales. The possible influence of ENSO at the sub-decadal precipitation variability of the studied area is explored in this section. First we ascertained that coherence and common power of the RPC1,2 series with ENSO are better resolved through the SOI than through the Niño-3.4 index, not only in the sub-decadal, but also at the longer scales. The SOI phases and the power distribution in the time-scale domain are illustrated in Fig.6a, where the ENSO's inherent quasi-biennial (or QB) and the so-called 'low-frequency' (or LF) modes becomes pronounced in the years of exceptionally strong El Niño/La Niña episodes. The significant variability modes of the RPC1,2 series are further projected on SOI's power spectrum (green and blue lines in Fig.6a).

Coherence *and* common power with SOI at the QB and LF bands were detected in the monthly and particularly in the *winter* RPC1, 2 series. These relations are best resolved in the observed variability of Taranto and Zakynthos stations, which cases are examined below.

The precipitation variability in *Taranto* reveals significant relation with SOI in terms of coherence *and* common power, mostly during the exceptional ENSO activity period of the late-1960s to the 2000s (where the Taranto modes at 1.9 and 4.9 years also prevailed). In particular, significant coherence is found between the *winter* series during three intervals (1965–72, 1980–82, and 1991–97) where strong El Niño episodes were evolving, with $\delta\varphi$ tending either to an *in-phase* or an *anti-phase* position (Fig.6b). On the other hand, the sub-decadal variability in the southern Greek Ionian stations also reveals three periods of significant relations with SOI, two of them at 5–9 years (from the early 1900s to the mid-1920s, and during the 1940s, which is however a low credibility interval for these stations), and third, at the QB band after the mid-1990s (Fig.6c). The strongest relation was detected during the first interval of ENSO activity, where a precipitation mode at 7 years also prevailed in the southern Greek Ionian region. In the characteristic case of Zakynthos station, this mode reveals strong relation with SOI from the early 1900s to the mid-1920s, both in terms of significant coherence (with $\delta\varphi$ tending to -90°) *and* common power (Fig.6d,e). This relation is still traced -but considerably weakened- northwards in Corfu station at 4 years and at 7 years.

4.2.1.2. ENSO related effects at the decadal scales. ENSO decadal and interdecadal variability (also referred as the Interdecadal Pacific Oscillation or IPO; Salinger et al., 2001; Brönnimann, 2007) prevails in SOI as an enhanced component prior the mid-1920s, and as a significant decadal mode after the early 1970s (Fig.6a). This variability has been proposed to be an ENSO inherent mode (Folland et al., 2002; Cobb et al., 2003) or a modulation of the sub-decadal modes (Gershunov and Barnett, 1998; Power et al., 1999) or a modulator process of the protracted El Niño and La Niña events when appropriate

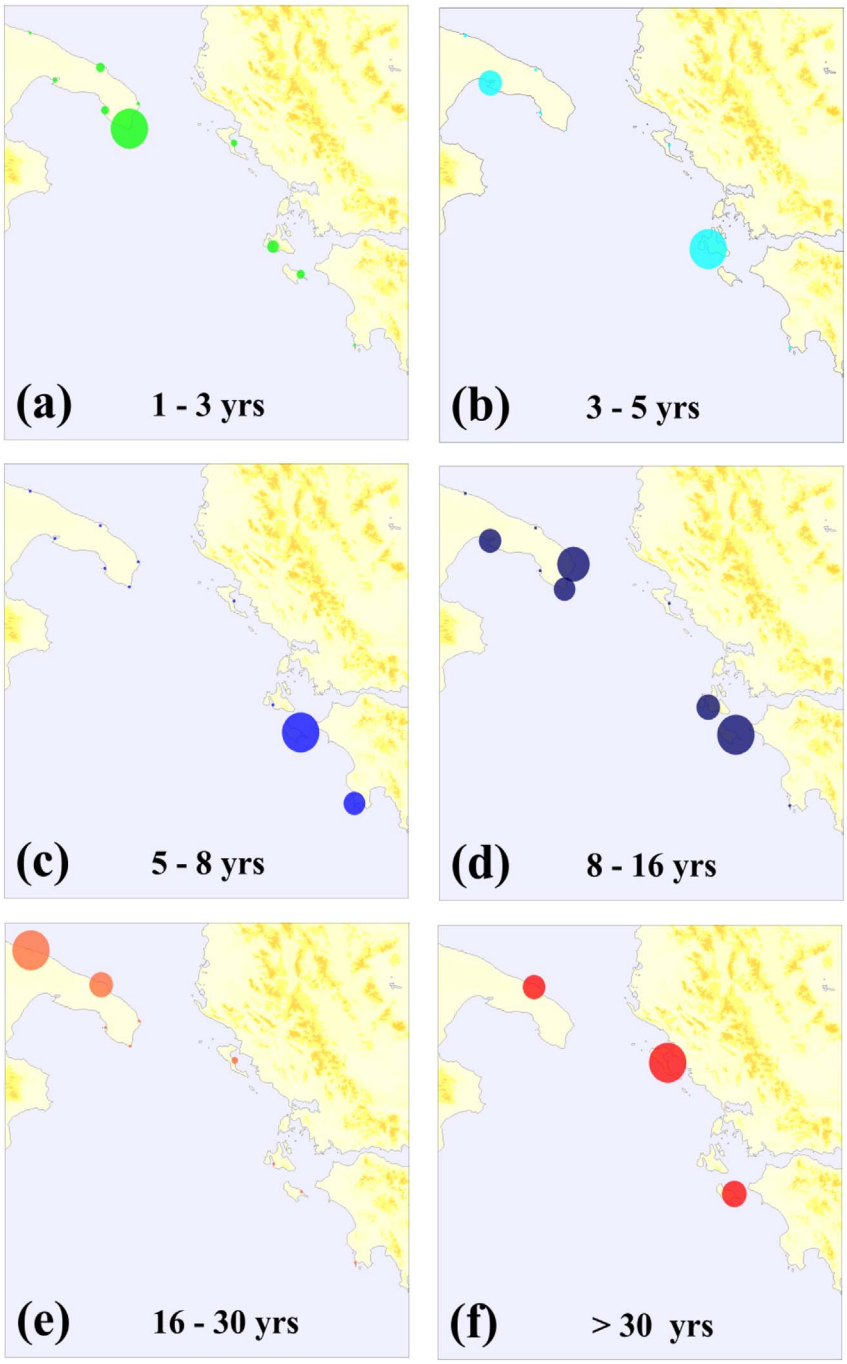

Fig. 5. Spatial distribution of the excessive spectral power $\mathcal{P}_{E,k}$ of the significant SSA modes (the radii of the circles are proportional to the $\mathcal{P}_{E,k}$ value), depicted according to their time-scales as indicated in each panel.

phasing exists with the QB and LF components (Allan and D'Arrigo, 1999; Allan, 2000) or finally, the signature of the Pacific Decadal Oscillation (Mantua et al., 1997).

Regarding the possible relation of the exceptional Otranto decadal precipitation mode with ENSO, it is first noticed that its development precedes the onset -at the 1970s- of the corresponding SOI activity by some decades, while no consistent frequency relation or coherence was traced before the 1970s. However, after the mid-1970s a significant relation of increasing strength detected in terms of both, coherence (with $\delta\varphi \cong -90^{\circ}$) *and* common power between the *winter* series (in the *monthly* series this relation appears only after the 1990s). A similar coherent relation also found between the *winter* precipitation variability of the other stations in the Adriatic side of Puglia and SOI, but without any significant impact on the corresponding precipitation heights. As will be seen later (in Section 4.2.3) strong EA effects also influence the precipitation variability there after the 1970s.

Unlike the Otranto case, the appearance of the strong decadal modes in the Taranto Gulf and the southern Greek Ionian region (particularly in *Taranto* and *Zakynthos* stations) in the early 1970s was almost concurrent with the onset of SOI's decadal mode and with the time where ENSO was entering a high activity epoch (started with the strong La Niña episode of 1973–75; Fig.6b,c). The amplitude variations of these modes are shown in Fig.7a,e, while the time evolution of their coherence and relative phases with SOI are depicted in Fig.7b,f. As can be seen there, the decadal precipitation variability in Zakynthos becomes highly coherent with SOI especially during the first period of ENSO activity (prior 1925), with $\delta\varphi$ stabilized at $-11^{\circ} \pm 14^{\circ}$. Afterwards this relation fades, but significant coherence *and* common power re-appears between 1970 and 1990 in the *winter* series (also traced northwards in Corfu area). Simultaneously, the 11.9 years mode in

Table 3
Pearson's linear correlation coefficient between the monthly or the extended winter (DJFM) precipitation series RPC1,2 and the climatic indices listed in the first column. Statistically significant correlations at the 90% confidence level are shown by bolded values, while those at 95% and 99% are indicated by yellow and orange shaded cells, respectively.

Climatic Index		Time Period	MONTHLY		D J F M	
			RPC-1	RPC-2	RPC-1	RPC-2
ATMOSPHERIC	S O I	1921-2010	0.04	0.13	0.11	0.14
	NAO HSt	1921-2010	**–0.31**	–0.09	0.12	**–0.25**
	E A	1950-2010	–0.20	0.04	–0.08	**–0.26**
	SCAND	1950-2010	**0.49**	–0.14	**0.51**	**0.23**
	EA – WR	1950-2010	0.04	–0.12	–0.06	**–0.29**
	Q B O	1948-2010	0.05	–0.09	0.06	–0.03
SST	ENSO 3.4	1950-2010	0.03	–0.09	–0.01	–0.13
	A M O	1921-2010	0.12	0.04	–0.03	0.18

Taranto becomes highly coherent with SOI, $\delta\varphi$ stabilizes to $-102^\circ \pm 11^\circ$ (Fig.7f) and the $\delta\varphi_c$ distribution is strongly unimodal (similarly to the Greek Ionian region, this relation becomes more prominent in the *winter* series). Additionally, in both periods the frequencies of these precipitation modes show a gradual convergence to SOI's frequency, with the difference remaining bounded to within 6% for Zakynthos and 12% for Taranto (Fig.7c,g). The corresponding phase relations, in reference to the frequency of the evolving SOI mode, are also shown in Fig.7d,h. Another prominent case of significant *anti-phase* coherence with SOI at the decadal scale after the mid-1980s in the Taranto Gulf (manifested in *Gallipoli*) will be examined below as a part of the bi-decadal variability.

4.2.1.3. ENSO related effects at the interdecadal scales. Two variability modes prevail at the interdecadal scales in SOI (Fig.6a): a strong but not significant *bi-decadal component* from the late 1930s to the 1980s, and a multidecadal fluctuation from the beginning of the 20th century (significant since the 1950s) at the scales longer than 40 years. None of these modes was found to be significant at the 0.05 level in the *winter* SOI.

The precipitation variability in the Greek Ionian region does not reveal any considerable relation with SOI at the bi-decadal scales while on the contrary, significant relations were found in Puglia from the early 1930s to the mid-1980s (best resolved in *Brindisi* and *Gallipoli*). The local modes at 21 years were found to be timely synchronized with SOI (Fig.8a,e), while the frequency and amplitude evolution of the *Brindisi* mode seems to follow SOI variations (Fig.8b,c), with $\delta\varphi$ tending to $46^\circ \pm 12^\circ$ (Fig.8d) and the $\delta\varphi_c$ distribution being unimodal. As a result, the bi-decadal variability in Brindisi reveals highly significant *nearly in-phase* coherence *and* common power with SOI, while a similar relation was also detected in Bari. In the southern Adriatic station of Otranto, significant out-of-phase ($\delta\varphi \cong 90^\circ$) coherence was found from 1920 to the mid-1960s but without common power (possibly indicating the low response of Otranto precipitation to bi-decadal forcing).

After the late-1960s, as the bi-decadal activity of the *monthly* SOI progressively fades, the Brindisi mode evolves in a rather similar way (and almost a constant 5:4 ratio is retained between the frequencies of these modes, as seen in Fig.8c), so that coherence fades-out in the early 1990s. However, as during the mid-1970s exceptional ENSO activity prevails at the decadal and the QB, LF scales, a new period of significant *anti-phase* coherence ($\delta\varphi \cong -90^\circ$ to -140°) with SOI emerges at the 10–13 years band (yet, without significant common power). This relation becomes again more pronounced in the Taranto Gulf side of Puglia, particularly in *Gallipoli* where the local bi-decadal mode reveals exceptionally high coherence with SOI (Fig.8f,h) *and* common power from the mid-1930s to the mid-1980s, while the $\delta\varphi_c$ distribution is unimodal. But remarkably, as the ENSO decadal activity emerges at the late-1960s, a strong *decadal* mode also appears in the precipitation of Gallipoli (Fig.8e) whose frequency evolution follows SOI, while $\delta\varphi$ stabilizes to $-138^\circ \pm 5^\circ$ (Fig.8g,h). Consequently, highly significant *anti-phase* coherence *and* common power emerges. Actually, this remarkable relation is part of the strong coupling found earlier (Section 4.2.1.2) at the same scales and epoch (mid-1980s to the 2000s) in the Taranto Gulf.

Finally, the relation of the observed precipitation variability with ENSO at the *multidecadal* scales ($s > 30$ years) was possible to be searched only for the Greek Ionian stations where appropriately long records were available (so that, $s_M = 42$–44 years). Significant *in-phase* coherence *and* common power between the precipitation variations in these stations and SOI were detected at scales longer than 35 years,

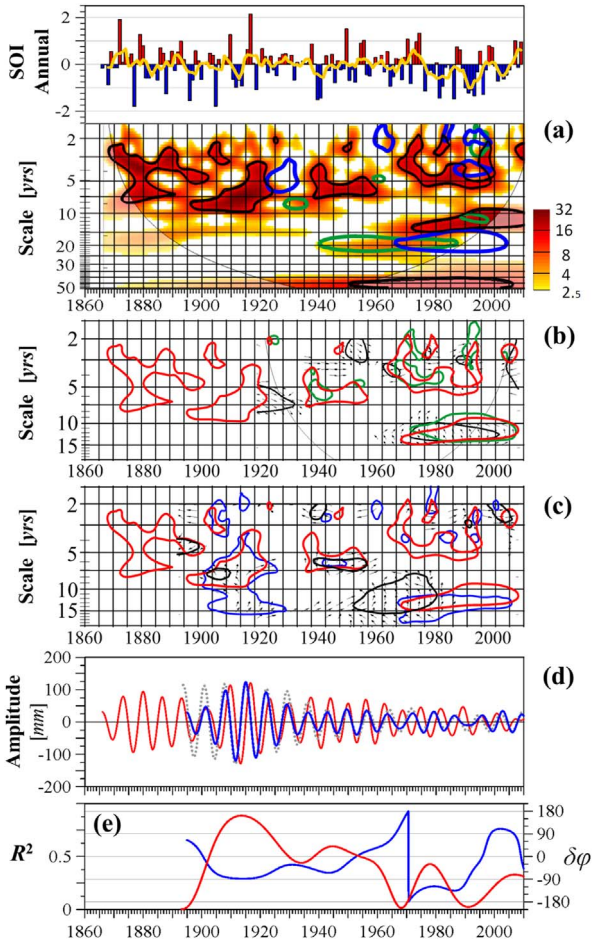

Fig. 6. (a):The *annual* SOI index (negative phases correspond to El Niño conditions) and the 5-years moving average (yellow curve) in the upper panel. The power distribution of the *monthly* SOI index at the time-scale domain is shown at the lower panel for levels higher than $2.5\sigma^2$. Regions of significant power of the RPC1 and RPC2 series are indicated by green and blue lines, respectively.
(b):Significant common power between the *monthly* precipitation in Taranto and SOI (green lines), along with regions of significant coherence between the corresponding *DJFM* series (black lines). The relative phases, $\delta\varphi$, are shown at the regions of enhanced or significant coherence by the small arrows according to the convention: "→" for $\delta\varphi = 0^\circ$, "↓" for $\delta\varphi = 90^\circ$, "←" for $\delta\varphi = 180^\circ$, "↑" for $\delta\varphi = 270^\circ$. To facilitate comparison, SOI's significant variability is also indicated by the red lines.
(c):As in panel 'b', but for Zakynthos station (blue curves now indicate the regions of significant common power).
(d):Amplitude evolution of Zakynthos precipitation mode at 7 years (blue curve for wavelets reconstruction, and dashed gray curve for SSA), compared with the corresponding component in the *monthly* SOI series (red curve, scale arbitrary).
(e):Evolution of the wavelet squared coherence R^2 (red curve, scale on the left) and of the cyclic phase difference $\delta\varphi_c$ (blue curve, scale on the right) between the modes depicted in 'd'. (For interpretation of the references to colour in this figure legend, the reader is referred to the web version of this article.)

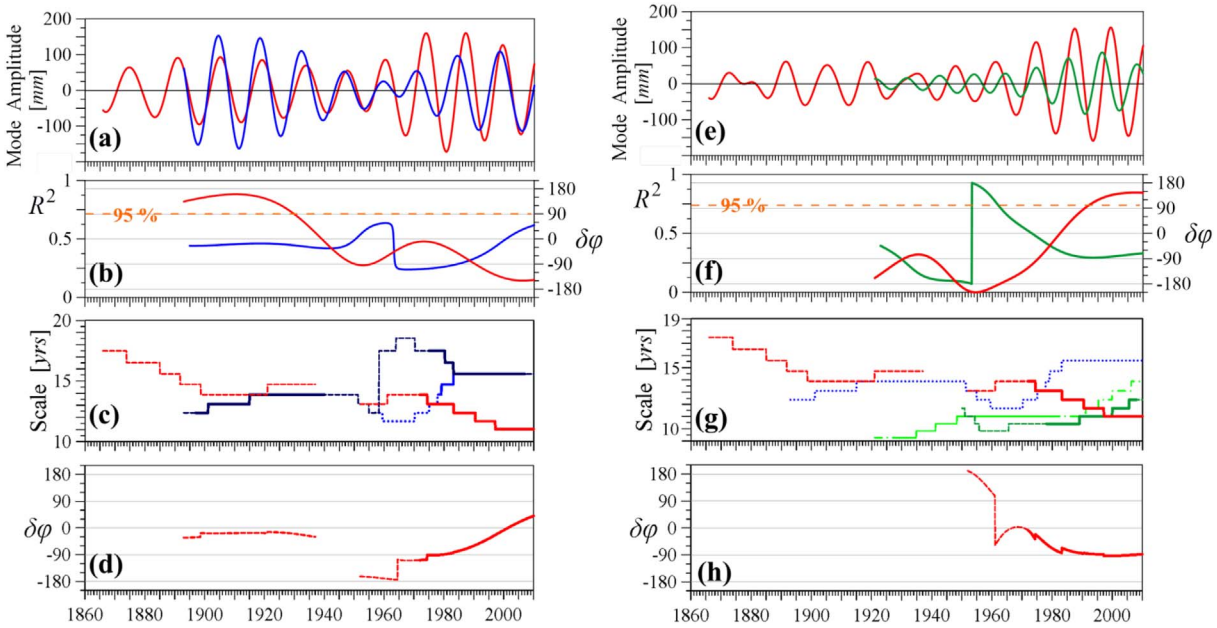

Fig. 7. (a,e): Amplitude evolution of the precipitation modes at 13.9 years in Zakynthos (blue curve in 'a'), at 11.9 years in Taranto (green curve in 'e'), and of the corresponding SOI component (red curve in both panels, scale arbitrary).
(b,f): Coherence R^2 (red curves) and $\delta\varphi_c$ variability (blue curve in 'b' and green in 'f') between the modes shown in (a) and (e). The dashed line indicates the 95% confidence level for R^2.
(c,g): Scale evolution of Zakynthos (blue line) and SOI (red line) decadal modes in 'c' (where a secondary mode appears between 1950 and 1985 at about 17 years). The evolution of the Taranto (green line) and SOI (red line) decadal modes are shown in panel 'g' (where the Otranto and Zakynthos modes are also depicted for comparison, by the light green and blue lines, respectively). Solid/dashed lines indicate statistically significant/non-significant periods for each mode.
(d,h): The phase relation $\delta\varphi_c$ between the decadal precipitation mode in Zakynthos (red curve in 'd') or Taranto (red curve in 'h') and SOI, in reference to SOI's evolving scales. Solid/dashed lines are as above. (For interpretation of the references to colour in this figure legend, the reader is referred to the web version of this article.)

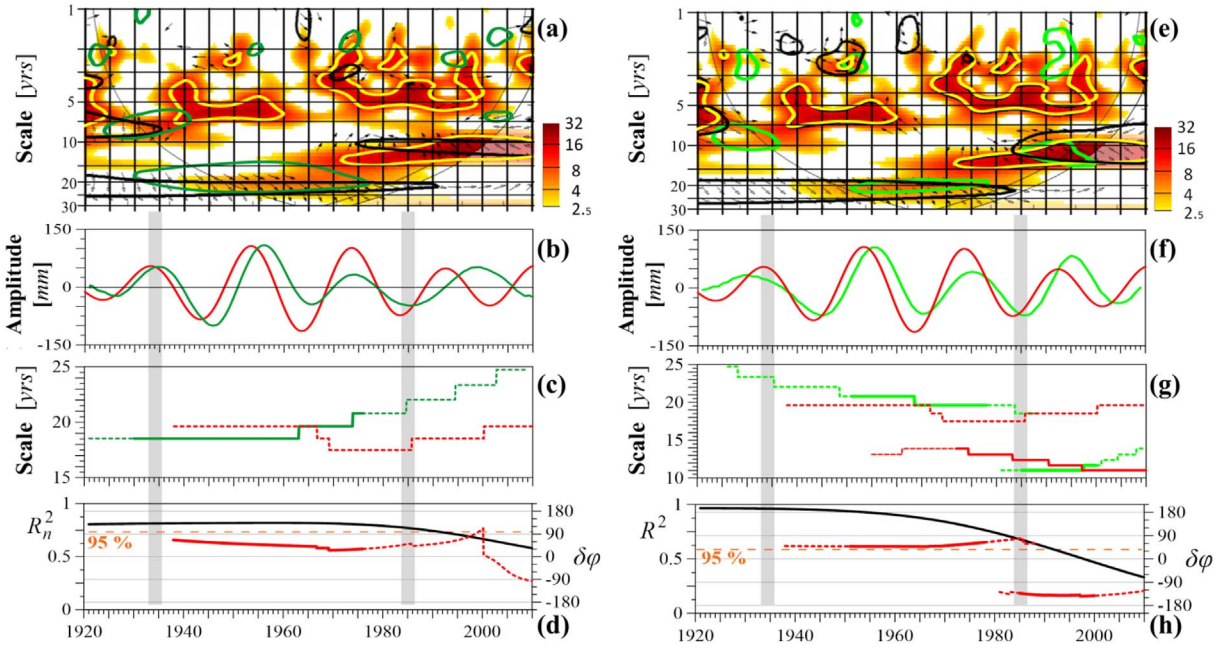

Fig. 8. (a, e): Significant power regions (green lines) of the precipitation series in Brindisi (a) and Gallipoli (e), projected for comparison on the power spectrum of the *monthly* SOI (shown for levels higher than $2.5\sigma^2$, with yellow lines indicating significant values). Regions of significant coherence are bordered by the black curves, along with $\delta\varphi$ arrows (according to the convention given in Fig.6).
(b, f): Amplitude evolution (green curves) of Brindisi (b) and Gallipoli (f) precipitation modes at 20.8 years, along with the corresponding component of the *monthly* SOI (red curves). The gray vertical strips approximately indicate the period of notable variance ($> 1\sigma^2$) in the SOI bi-decadal component.
(c, g): Scale evolution (green lines) of the bi-decadal modes in Brindisi (c), Gallipoli (g) and in *monthly* SOI (red lines). Solid/dashed lines indicate periods where each mode was significant/non-significant.
(d, h): Coherence R^2 (black curves) between the 20.8 years modes in Brindisi (d) or Gallipoli (h) and the bi-decadal SOI component (the 95% confidence level is indicated by the dashed orange lines). The corresponding $\delta\varphi_c$ variations in respect to SOI evolving scales are also depicted (red curves). Solid/dashed lines are as above. (For interpretation of the references to colour in this figure legend, the reader is referred to the web version of this article.)

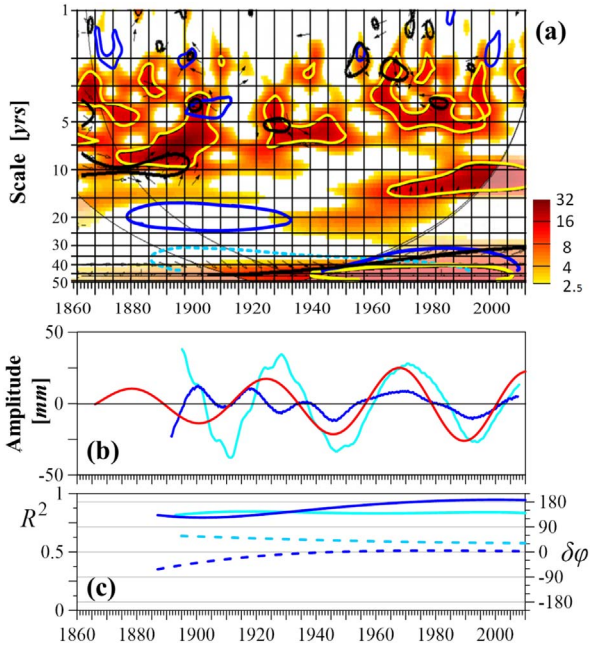

Fig. 9. (a): Significant power regions of Corfu precipitation series (blue lines) projected for comparison on the *monthly* SOI's spectrum (shown for levels higher than $2.5\sigma^2$, with the yellow lines indicating significant values). The regions of significant coherence are bordered by the black curves. The dashed cyan line for scales $s > 30$ years shows the region of significant power in Zakynthos precipitation series.
(b): The SSA multidecadal precipitation modes in Corfu (blue curve) and Zakynthos (cyan), and the *monthly* SOI component at 42 years (red curve).
(c): Evolution of the wavelet coherence R^2 between Corfu (solid blue curve) or Zakynthos (solid cyan curve) precipitation with the *monthly* SOI component, at 42 years. The corresponding relative phases $\delta\varphi$ are also depicted by the dashed blue curve for Corfu and by the dashed cyan curve for Zakynthos (scale on the right). (For interpretation of the references to colour in this figure legend, the reader is referred to the web version of this article.)

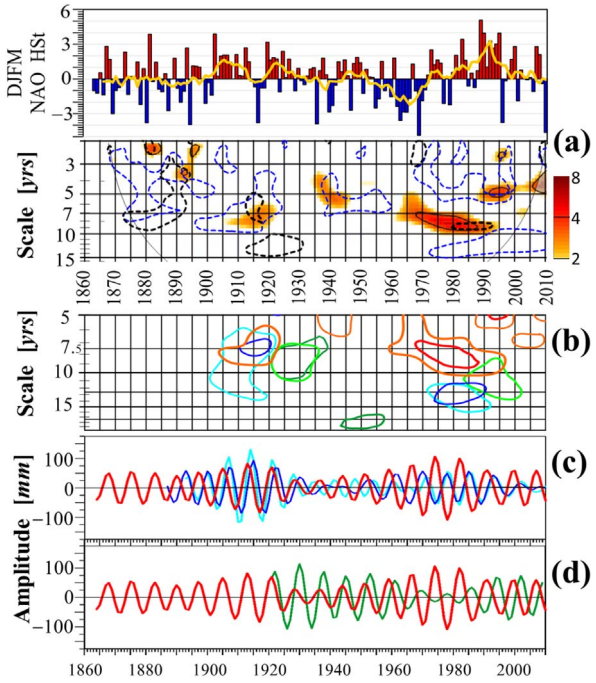

Fig. 10. (a): The extended *winter* (*DJFM*) NAO HSt index along with the 5-years moving average (yellow curve) is shown at the upper panel. The power distribution of the *winter* NAO HSt index for levels higher than $2\sigma^2$ is shown at the lower panel. Significant variance regions of the *monthly* NAO and SOI are also indicated by the dashed black and blue lines, respectively.
(b): Comparison of the significant power regions of the *winter* NAO HSt index (red curves, corresponding to $\sigma^2 = 3.5$) with those in the *winter* precipitation of Brindisi (dark green), Corfu (blue), Zakynthos (cyan), and RPC1 series (light green curves). Orange lines indicate the $\sigma^2 = 2.0$ variance level in the NAO index (also shown in 'a').
(c): Amplitude evolution of the *winter* precipitation mode at 7.6 years in Corfu (blue curve) and at 7 years in Zakynthos (cyan curve), in comparison with the *winter* NAO HSt component at 7.8 years (red curve).
(d): As in panel 'c', but for the *winter* (*DJFM*) precipitation variability mode at 7.6 years in Brindisi (green curve). (For interpretation of the references to colour in this figure legend, the reader is referred to the web version of this article.)

progressively intensifying since the beginning of the 20th century (Fig.9a). This relation is also reflected by the amplitude evolution of the slow SSA precipitation components at 42 years (Fig.9b), as well as by the high R^2 and the low $\delta\varphi$ values between the corresponding wavelet components and the SOI variability in this scale (Fig.9c). However, as it is indicated by the cone of interest (COI), reduced credibility attends the characteristics of the detected variability and the estimated relations in such long scales.

4.2.2. Relations with NAO

Among the adopted NAO indices (mentioned in Section 3.1) it was ascertained that NAO HSt better designates coherence and common power with the observed precipitation variability in the studied area (nevertheless, qualitatively limited differences emerged when the other NAO indices were considered).

4.2.2.1. NAO related effects at the sub-decadal scales. The extended winter (*DJFM*) NAO HSt index and its power distribution in the time-scale domain are illustrated for scales $s < 15$ years in Fig.10a. Both the RPC1 and RPC2 series were found to reveal distinct epochs of enhanced coherence *and* common power with the *winter* NAO HSt index at the sub-decadal scales. The underlying relations are best discerned in the *winter* series of *Brindisi*, *Corfu*, and *Zakynthos*, whose amplitude evolution at 7–8 years are compared with NAO variability in Fig.10b–d. As can be seen there, during the 1900–1925 period where *positive* phases dominate in NAO, the 7–8 years modes in the Greek Ionian stations reveals significant coherence with $\delta\varphi \cong 30^\circ$–$90^\circ$ (Fig.10c). From the 1930s to the 1960s, where NAO reveals mixed phases and its activity at 7–8 years fades (Fig.10a), the corresponding *winter* precipitation variability in the Greek Ionian region is reduced accordingly (Fig.10b,c). Then, besides the appearance of the NAO sub-decadal mode at 6–9 years from the 1960s to the 1990s, the winter variability in the Greek Ionian stations reveal enhanced -yet not significant- *anti-phase* coherence with NAO from the late 1960s to the late 1980s (Fig.10b). These remarks indicate that the sub-decadal modes of the winter precipitation at 7–7.6 years *tend to* prevail at least in parts of the studied area during periods of persistent strong positive NAO phases. *Under such circumstances these precipitation modes seem to be synchronized with* NAO and $\delta\varphi$ *tends to* 90°. During the intervals of persistent negative or even alternating phases of NAO, the 7–7.6 years modes fades and an *anti-phase* relation tends to settle. This behavior is compatible with the *weak* anti-correlation of the Central Mediterranean precipitation with NAO which is often detected by global correlation coefficients (as can be seen for example in Wanner et al., 2001; Luterbacher and Xoplaki, 2003; Hurrell et al., 2003) although strong coupling periods, as those indicated above, emerge. We further noticed that the relation strength seems to be dependent on ENSO state as has been suggested by many researchers (e.g., Huang et al., 1998; Mann and Bradley, 2000; Pozo-Vázquez et al., 2001; Knippertz et al., 2003; Mokhov and Smirnov, 2006; OrtizBevia et al., 2010). For example, during the 1910–1920 period where NAO variability at the sub-decadal scales is strongly related with ENSO (Fig.10a), its impacts on the precipitation of the studied area become locally strong, while during 1960–1995 the ENSO–NAO relation weakens and then NAO influence on the studied area fades accordingly.

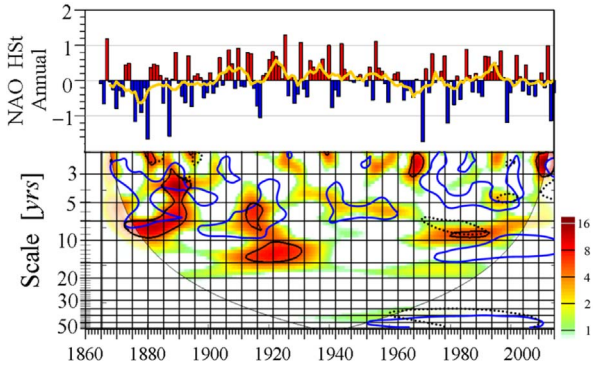

Fig. 11. The *annual* NAO HSt index, and the 7 years moving average (yellow curve) are shown at the upper panel. The power distribution of the *monthly* NAO HSt index (for levels higher than $1\sigma^2 = 3$) is shown at the lower panel. For comparison, the significant variance regions of the *winter* NAO HSt index and of the *monthly* SOI are indicated by the dotted black and the solid blue curves, respectively. (For interpretation of the references to colour in this figure legend, the reader is referred to the web version of this article.)

4.2.2.2. NAO related effects at the decadal scales. Because the *winter* NAO activity at the *decadal* and *quasi-decadal* scales is limited (Fig.10a), no statistically significant relation is found between the precipitation variability in the studied area and the *DJFM* index. Nevertheless, the *annual* NAO HSt index reveals three periods of strong variance at these scales, the first from the 1870s to the 1890s, the second from the early 1900s to the late 1930s (both being parts of NAO broad-band activity) and the third from the mid-1960s to the 2000s (Fig.11). The NAO variability in the first two periods is significantly correlated with SOI in terms of coherence *and* common power, while that in the third period *-which is the only one that was detected as significant in the winter* NAO *index - is not* correlated with SOI. Since NAO represents a winter season natural variability mode of the Northern Atlantic troposphere, the third period activity is considered as a NAO-inherent variation (e.g., Da Costa and Colin De Verdiere, 2002; Gámiz-Fortis et al., 2002; Paluš and Novotná, 2004; Feliks et al., 2010). On the contrary, the absence of winter NAO activity during the first (1870–1890) and the second (1900–1935) periods, combined with the significant relation with SOI, indicates a possible implication of ENSO in the modulation of the NAO variability during both periods. This possibility will be further searched below.

Since the precipitation data in Puglia are available after 1920, while the *monthly* NAO HSt index does not exhibit significant activity at the decadal scales after 1930–1935, no significant coherence is found in these scales. On the other hand, the significant decadal modes in the southern Greek Ionian region (at 13.9 years in Zakynthos and at 10.4 years in Cephalonia) from the early 1900s to the mid-1930s are concurrent and highly coherent with the second period of NAO variability (Fig.12a,b and e,f). In particular, during this period the frequency of the Cephalonian mode converges to NAO, $\delta\varphi$ stabilizes to $-86^\circ \pm 2.5^\circ$ and then, coherence reveals highly significant values (Fig.12c,d). Simultaneously, this mode was found to be coherent with SOI's decadal variability (however, the relation is weaker than with NAO), and additionally the frequency and amplitude evolution of the Cephalonian mode does not follow the corresponding variations in SOI (Fig.12b,c). Interestingly, during the same period, the evolution of the 13.9 years mode in the neighborhood southern Ionian station of Zakynthos reveals stronger relation with SOI than with NAO. This fact is first demonstrated in Fig.12f (where the amplitude evolution of these modes are compared) and subsequently in Fig.12g, where the frequency of the precipitation mode is seen to follow closely the drifting frequency of SOI (but not the increasing frequency of NAO). Furthermore, the onset of the 13.9 years precipitation mode is detected *prior* the appearance of NAO's decadal mode (Fig.12e,f).

Given the global-scale character of ENSO, the aforementioned coherent variations of the Greek Ionian region precipitation with both SOI and NAO at the same scales and period can be associated with: (a) two concurrent but *independent* activities, one in ENSO and another in NAO, or(b) a "reflection" through NAO of the ENSO activity, that presumably triggers a relevant variability in NAO. To discriminate between these two scenarios, the relationship of the relative phases $\delta\varphi_{N\text{-}Z}$ between NAO and the 13.9 years mode in Zakynthos (where $\delta\varphi_{N\text{-}Z} = -98^\circ \pm 5^\circ$; Fig.12h) should be examined in accordance to the relative phases $\delta\varphi_{S\text{-}Z}$ between the 13.9 years mode and SOI (where $\delta\varphi_{S\text{-}Z} = -11^\circ \pm 14^\circ$; Fig.7d). In case where the *transitive coupling relation* scenario (b) is valid, then the relative phases of the three unidirectionally coupled oscillators should verify the equation $\delta\varphi_{S\text{-}Z} - \delta\varphi_{N\text{-}Z} = \delta\varphi_{S\text{-}N}$ (where $\delta\varphi_{S\text{-}N}$ represents the relative phase between SOI and NAO at the decadal scales), which anticipates $\delta\varphi_{S\text{-}N} \cong 87^\circ \pm 19^\circ$. The relevant analysis revealed the existence of an enhanced and well-defined (but not-significant at the 0.05 level) coherence between the *monthly* SOI and the NAO HSt series during 1905–1935, with the relative phases being equal to $\delta\varphi_{S\text{-}N} = 77^\circ$ ($\pm 10^\circ$). This outcome verifies in the statistical sense the validity of the equation $\delta\varphi_{S\text{-}Z} - \delta\varphi_{N\text{-}Z} = \delta\varphi_{S\text{-}N}$ and indicates that the simultaneous strong relation of the quasi-decadal precipitation variability in the southern Greek Ionian region with both the non-significant SOI activity and the significant mode in *monthly* NAO, was probably a result of NAO variability that was actually induced by ENSO, rather than the direct impact of a NAO-inherent mode.

4.2.2.3. NAO related effects at the interdecadal scales. As can be seen in Fig. 13a, the *winter* NAO HSt index exhibits enhanced, but not significant activity at 20–25 years from the early 1900s to the early 1960s. However, significant activity prevails from the mid-1950s to the 2000s at 40–50 years, associated with the NAO multidecadal fluctuation from negative to positive phases during this period (actually, this fluctuation seems to be part of a significant slow mode in NAO, which is detected by SSA and MTM between 65 and 85 years). The *winter* NAO bi-decadal variations reveal *in-phase* coherence with SOI from the late 1930s to the late 1990s (significant from 1955 to 1985), but no common power. Moreover, the multidecadal NAO fluctuation reveals significant *anti-phase* coherence with SOI along the entire observational period (Figs. 11 and 13a) while significant common power appears only after the mid-1940s.

In this framework, it was found that the strong *bi-decadal* precipitation modes in the Adriatic side of Puglia at 21 years and 28 years, reveal only limited relation with the *winter* NAO HSt index (mostly traced in Brindisi from the late 1930s to the late 1960s). On the other hand, the corresponding variability in the Greek Ionian region reveals two periods of significant *anti-phase* coherence with the *winter* NAO, the first from the 1890s to the late 1930s, and the second from the 1960s to the 2000s (Fig.13b,c). Although none of these relations entangles significant components (at the 0.05 level), it is noteworthy that *coherence at the bi-decadal scales is much stronger in the northern part of the Greek Ionian region than in the southern part* where the effects of ENSO (discussed in Section 4.2.1.3) dominate over those of NAO at the quasi-decadal scales, with the transitional regime spotted in the area of Cephalonia.

Finally, regarding the *multidecadal scales* ($s > 30$ years), the precipitation in the Greek Ionian stations reveal significant *anti-phase* coherence with the *winter* NAO along the entire observational period (Fig.13b,c) *and* significant common power since the 1950s. This relation is also prominent in the amplitude evolution of the corresponding modes (Fig.13d,f), while it is partially reflected in the global correlation coefficient r_P of the RPC2 series (Table 3). The frequency evolution of these modes follows closely the corresponding variations of NAO especially in the southern Greek Ionian region (Fig.13e,g). However, as indicated by COI, these results should be considered under the precaution of the reduced credibility implied by the edge effects entangled in such long scales.

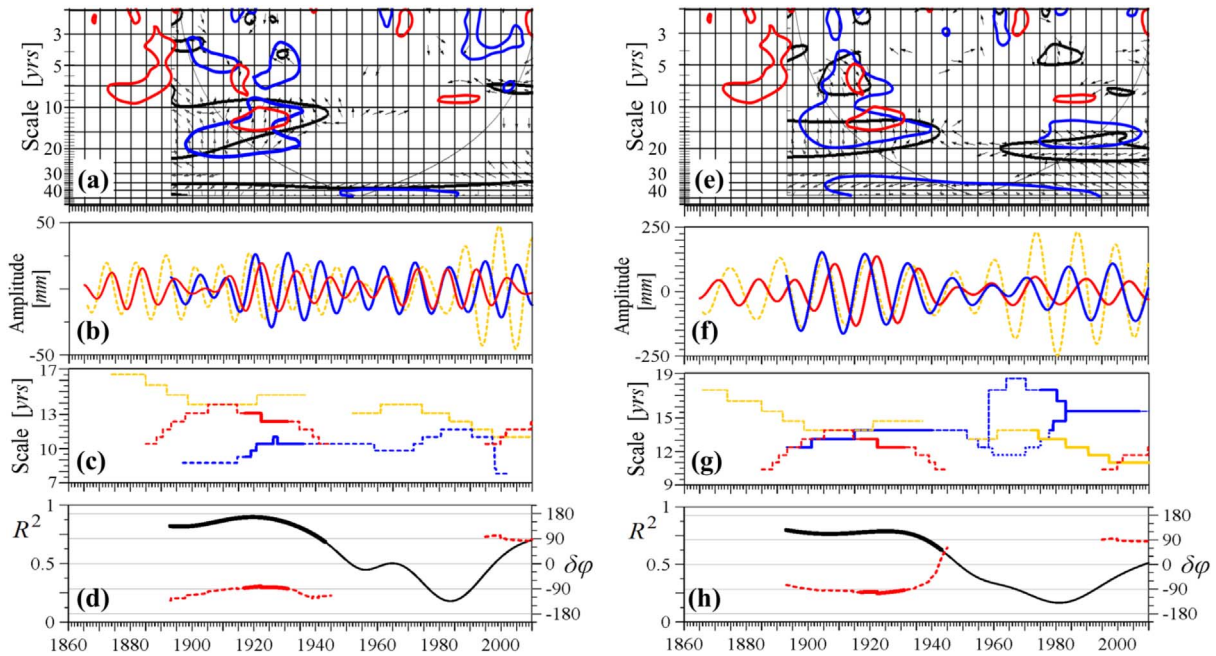

Fig. 12. (a,e): Significant power regions of the precipitation series in Cephalonia and Zakynthos (blue lines in 'a' and 'e', respectively) and of the *monthly* NAO HSt index (red lines). Significant coherence with NAO is bordered by the bolded black curves, while $\delta\varphi$ arrows indicate the relative phases (according to the convention given in Fig.6).
(b,f): Amplitude evolution (blue curves) of the 10.4 years mode in Cephalonia (b) and of the 13.9 years mode in Zakynthos (f). For comparison the *monthly* NAO HSt (red curve) and the SOI mode (yellow dashed curve) are shown at 10.4 years in 'b' and at 13.9 years in 'f'.
(c,g): Scales evolution of the *monthly* NAO HSt index (red line) and of the decadal modes (blue lines) in Cephalonia (c) and Zakynthos (g). For comparison, the evolution of the decadal SOI mode is also depicted (yellow lines). Solid/dashed lines indicate periods where each mode was significant/non-significant.
(d,h): Coherence R^2 (black curves) between the decadal modes in Cephalonia (d) or Zakynthos (h) and the *monthly* NAO. The $\delta\varphi_c$ variations (red curves) are also depicted, in reference to the evolving NAO scales. Solid/dashed lines are as above. (For interpretation of the references to colour in this figure legend, the reader is referred to the web version of this article.)

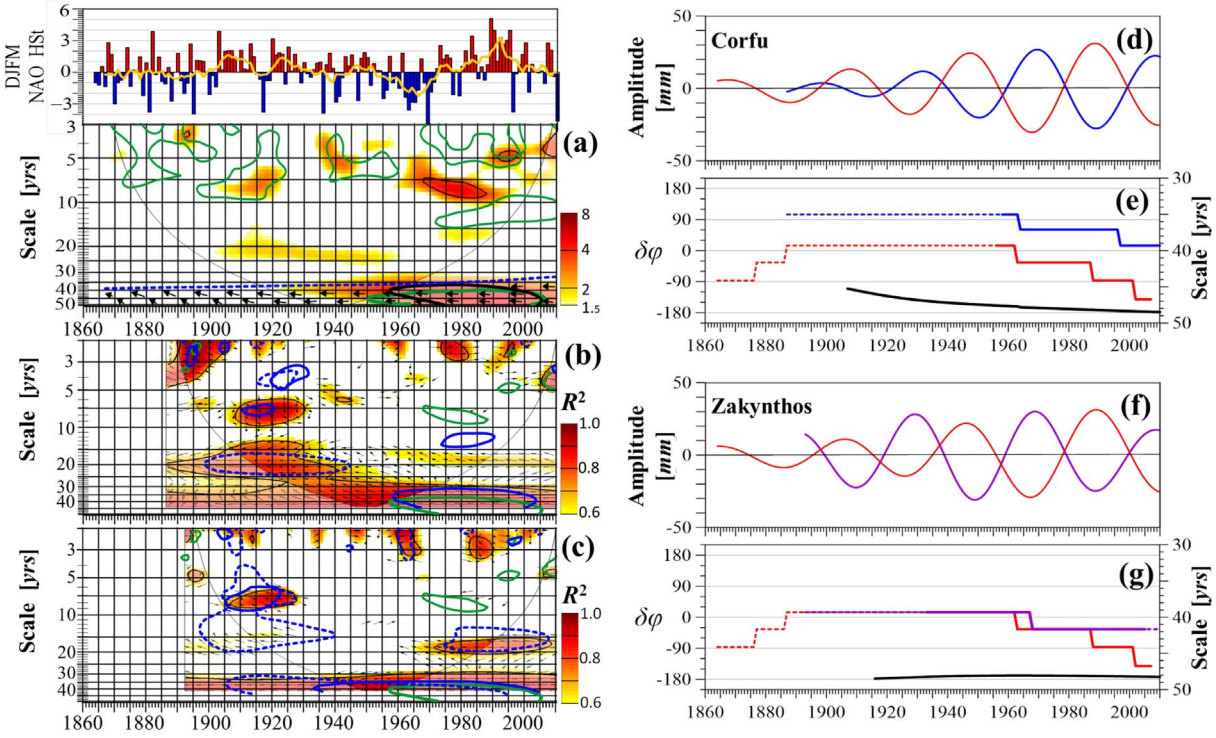

Fig. 13. (a): The extended *winter* (*DJFM*) NAO HSt index along with the 7-years moving average (upper panel) and its power distribution for levels higher than $1.5\sigma^2$ (lower panel). For comparison, the significant power regions of the *monthly* SOI are also shown (green lines). Regions of significant coherence between the *winter* SOI and NAO HSt are further indicated by the dashed blue line, for scales $s \geq 30$ years.
(b,c): Coherence of the *winter* precipitation in Corfu (b) or Zakynthos (c) with NAO, shown only for $R^2 \geq 0.6$ (while significant values are indicated by black curves). The significant power regions for the winter/monthly series of Corfu and Zakynthos series are bordered by the solid/dashed blue curves respectively, and those for the *winter* NAO by the green curves.
(d,e): The multidecadal *winter* precipitation components in Corfu (blue curve) and in NAO HSt (red curve) are shown in panel 'd'. Their scale evolution is accordingly depicted in (e), along with the $\delta\varphi_c$ variations (black curves). Solid/dashed lines indicate significant/non-significant periods in each mode.
(f,g): As above, but for Zakynthos station.

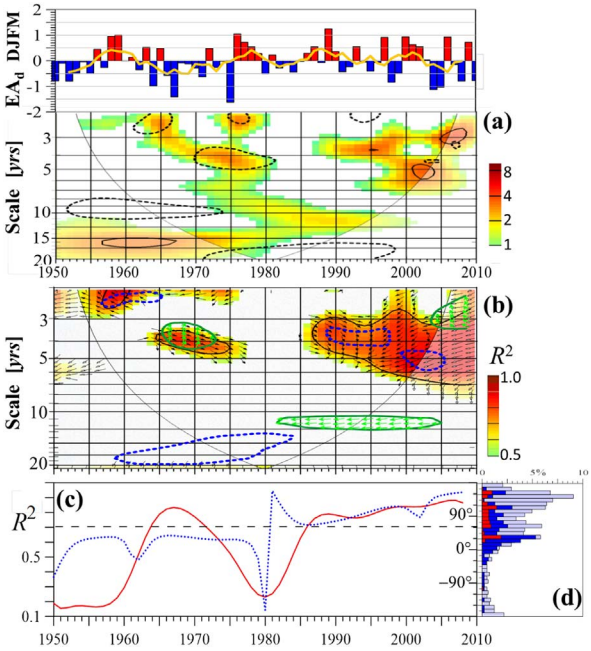

Fig. 14. (a): The *DJFM* EA_d index and the 5-years moving average (yellow curve) are shown at the upper panel. Power distribution of the *winter* EA_d index is shown for levels higher than $1\sigma^2$ at the lower panel. Significant power regions of the *monthly* EA_d index are also depicted by the dashed lines.
(b): Coherence of the *winter* RPC2 series with the EA_d index (for $R^2 > 0.5$), and regions of significant common power (dashed blue curves). The corresponding regions for the *winter* RPC1 series are also indicated by the green curves.
(c): Coherence R^2 evolution (red curve) between the *winter* RPC2 and EA_d at 3.8 years, along with the corresponding $\delta\varphi_c$ variations (dotted blue curve).
(d): Frequency distribution of $\delta\varphi_c$ between the RPC2 and EA_d over the 3–7 years band (gray bars), over the 3.6–4 years band (blue bars), and over the periods of significant coherence (red bars). (For interpretation of the references to colour in this figure legend, the reader is referred to the web version of this article.)

4.2.3. Relations with EA

A preliminary analysis showed that the relationship of the precipitation variability in the studied area with EA is more effectively resolved in the *winter* series. Because the EA index reveals a strong secular trend, the detrended index (EA_d) was used in the subsequent analysis. The phases of EA_d and its significant variability in the time-scale domain are shown in Fig.14a. As it is seen there, the *winter* index spends longer intervals during a given –mostly negative- phase from 1950 to the late-1970s than after the 1980s where frequent phase alternations prevail. As a result, during the first period significant EA_d activity is detected at the 14–18 years band, which subsequently drifts to the decadal scales and progressively fades. In the second period (after the 1980s) significant EA_d activity is found to the short scales. In the transitional interval (at about the 1970s) the *winter* EA_d reveals a broad-band, strong but no significant variability, which is actually the imprint of a corresponding activity in the *monthly* index. Besides an apparent timing of EA variability with the periods of persistent NAO phases, the *winter* EA_d index is not correlated with NAO but instead, it reveals significant coherence *and* common power with the *winter* SOI at the 3–6 years band (from the mid-1960 to the late-1970s) and at the 10–15 years band (from the 1980s to the 1990s).

In this framework, the *winter* RPC2 series (that represents the *DJFM* precipitation variability in the Greek Ionian region) was found to be strongly correlated with the *winter* EA_d at the 3–7 years band in terms of significant coherence *and* common power, first from 1950 to the mid-1970s, and then, from the mid-1980s to 2010 (Fig.14b). Significant precipitation modes have been found in the studied area at these scales, such as the 3.8 years mode in Cephalonia. The relation of the *winter* RPC2 series with EA_d at 3.8 years shows an epoch of stable *in-phase* ($\delta\varphi \cong 30^\circ$) coherence until the late-1970s (Fig.14c). Then, coherence is lost during a short interval and $\delta\varphi$ lags abruptly by almost 360°, while it re-establishes after the late 1980s at a roughly *anti-phase* state ($\delta\varphi_c \cong 150^\circ$). Due to these transitions, the $\delta\varphi_c$ distribution over the 3–7 years band reveals two peaks at 30°, 60° and a global maximum at 150°, each one reflecting the residence time of the *winter* RPC2 series in the corresponding phases (Fig.14d). The overall maximum at 150° explains the *anti-phase* relation indicated by the highly negative r_P value in Table 3. Apart from the sub-decadal scales, the *winter* RPC2 series reveals significant common power with EA_d at 13–20 years, between the 1960s and the mid-1980s (Fig.14b) but without any coherence.

Similarly to the Greek Ionian region, the *winter* RPC1 series reveals out-of-phase ($\delta\varphi \cong -90^\circ$) coherence *and* common power with EA_d at the sub-decadal scales from 1950 to the mid-1970s (Fig.14b). Afterwards, this relation weakens, but significant *anti-phase* coherence *and* common power prevail at the decadal scales (mostly seen in the *winter* precipitation of the Taranto Gulf stations at 11–13 years, from the early 1980s to the late 1990s). Although this fact indicates a strong coupling with the EA pattern, the ENSO activity seems to have a rather important implication, as during the same period, the decadal precipitation modes in Puglia (e.g., the 11.9 years mode in Taranto) found earlier to reveal highly coherent variations with SOI (Fig.7e–h). At the same time, a transitive coupling relation seems to exist between ENSO and EA, as the EA_d variations reveal significant coherence (with $\delta\varphi \cong 90^\circ$) *and* common power with SOI.

On the other hand, the exceptional precipitation mode at 10.4 years in *Otranto* area reveals significant *in-phase* coherence *and* common power with the *monthly* EA_d index until the late 1970s (barely seen in

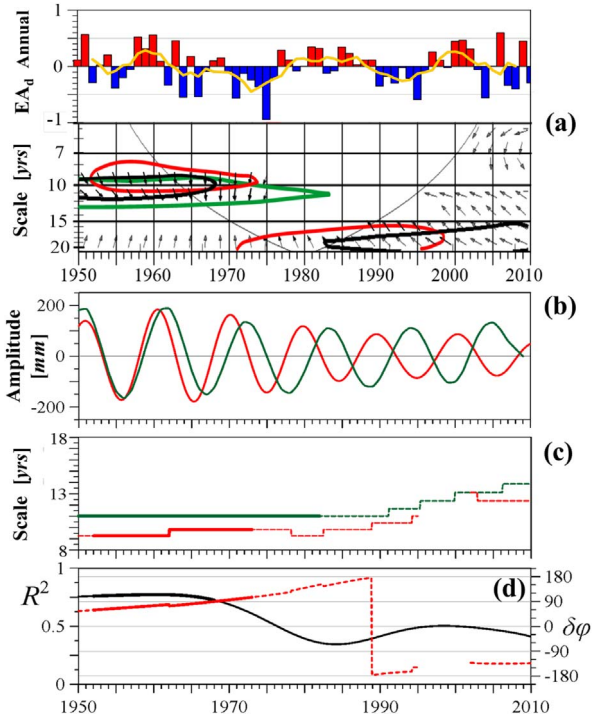

Fig. 15. (a): The *annual* EA_d index and the 5-years moving average (yellow curve) are shown at the upper panel. Significant power regions of the Otranto *monthly* precipitation and of the EA_d index are shown in the lower panel by the green and red lines respectively, while significant coherence regions are bordered by the bolded black lines.
(b): Amplitude evolution of the Otranto 10.4 years mode (green curve) and of the corresponding *monthly* EA_d component (red curve).
(c): Scale evolution of the Otranto (green curve) and the EA_d (red curve) decadal modes. Solid/dashed lines indicate significant/non-significant periods in each mode.
(d): Coherence R^2 evolution (black curve) between the Otranto and EA_d decadal modes. The corresponding $\delta\varphi_c$ variations (red curve) are given in respect to the EA_d scales (solid/dashed lines are as above). (For interpretation of the references to colour in this figure legend, the reader is referred to the web version of this article.)

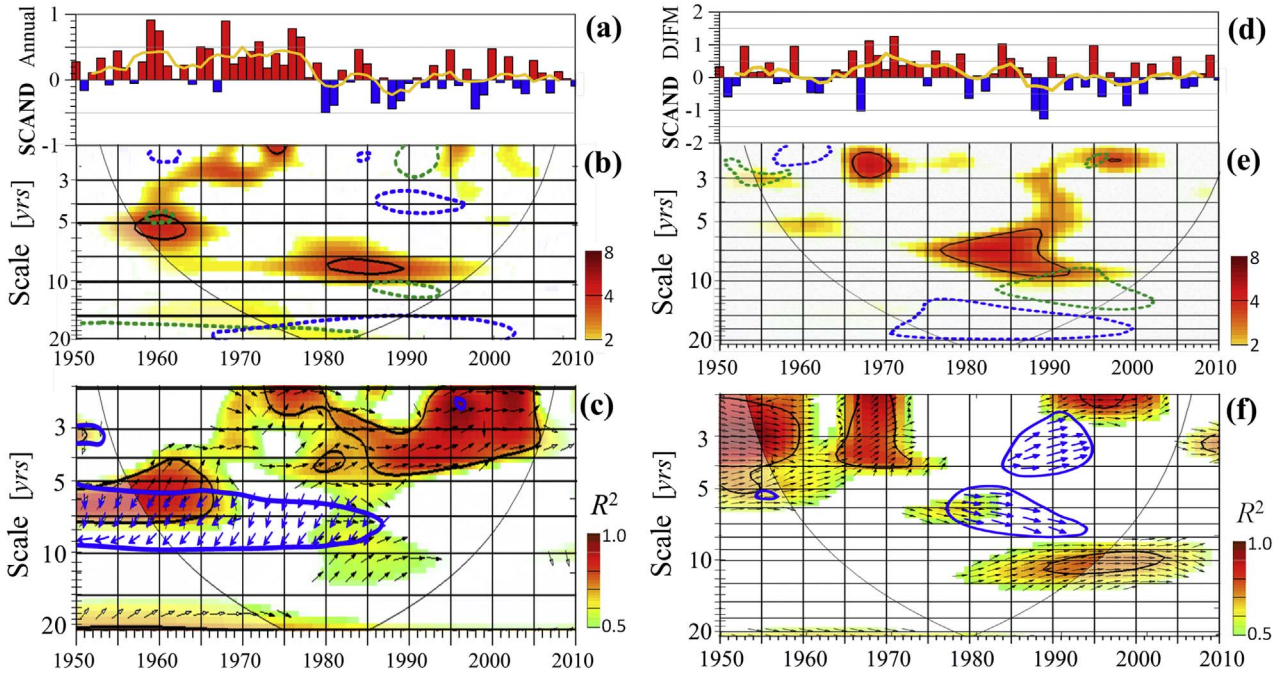

Fig. 16. (a,d): Phases of the *annual* (a) and *winter* (d) SCAND index, along with the 5-years moving averages (yellow curves).
(b,e): Power distribution of the *monthly* (b) and *winter* (e) SCAND index (shown only for levels higher than $2\sigma^2$). Significant power regions of the corresponding RPC1 and RPC2 series are respectively indicated by the dotted green and blue lines.
(c,f): Coherence regions of the *monthly* (c) and the *winter* (f) RPC1 series with the corresponding SCAND indices (shown only for $R^2 > 0.5$). The corresponding regions for RPC2 series are indicated by the blue curves along with the relative phases $\delta\varphi$ (blue arrows, according to the convention given in Fig.6). (For interpretation of the references to colour in this figure legend, the reader is referred to the web version of this article.)

the *winter* series). At the early 1980s where the decadal variability in the *monthly* EA_d fades, coherence reduces and the 10.4 years mode weakens notably (Fig.15a,b,d). Nevertheless, the decadal EA mode remains in the *winter* season as a strong but not significant component (which is related with ENSO as was mentioned above) and the *winter* precipitation in Otranto retains significant *anti-phase* coherence *and* common power with this mode. This relation is also traced in the *monthly* series, while the frequency of the Otranto mode remains close to that of the EA_d decadal mode (Fig.15c,d). Hence, it seems that *the maintenance of the enhanced precipitation variance in Otranto after the early* 1980s *is mostly due to the winter season* EA *variability*. A similar relation was further found for the *winter* precipitation of the other Adriatic stations (mostly pronounced in Bari after the 1980s).

4.2.4. Relations with SCAND

The *annual* and *winter* SCAND indices are respectively shown in Fig.16a,d. *Positive* phases which strongly enhance the Mediterranean cyclogenesis, the sirocco-type southern circulation, and the precipitation in the Central Mediterranean (Xoplaki, 2002; Ulbrich et al., 2012) represent the dominant state of SCAND, particularly from the 1950 to the late-1970s. During this period, significant variability is detected at the sub-decadal scales ($s < 7$ years), which is however restricted in the *winter* index (Fig.16b,e). Afterwards, from the late 1970s to the 2000s, the SCAND index reveals continuous phase alternations mainly associated with the *winter* season variability, reflected in the time-scale domain as significant activity at the 6–9 years band (Fig.16e).

In this framework, it was found that the major part of the studied area is strongly influenced by the SCAND variations. Both the *monthly* RPC1 and RPC2 series reveal significant *in-phase* coherence *and* common power with SCAND in two periods: one prior to the 1970s at scales $s < 5$ years (more pronounced in the *monthly* series), and another after the mid-1970s at the short (2–4 years) and the decadal (8–12 years) scales. The first period is mostly associated with the short-scale variability of the *monthly* SCAND index during the persistent positive phases, while the second is related with the additional prevalence of decadal scale fluctuations mostly in the *winter* index (Fig.16b,e). This relation is considerably stronger in the Taranto Gulf side where *the coupling* with SCAND in the sub-decadal scales reveals characteristics of transient *fp*-type synchronization events, *and accounts for the major part of the* 2.3 *years variability in Leuca*. Significant *in-phase* relation is also detected there with the *winter* SCAND index at the decadal scales, from the late 1970s to the 2000s. This relation fades towards the Adriatic, with the *winter* decadal variability in Otranto indicating a transition from the SCAND-influenced area of the Taranto Gulf to the EA-influenced area of the Adriatic coast. The effects of the *winter* SCAND on the maintenance of the Otranto's decadal mode after the 1980s are rather limited, compared to those of EA. Implications of NAO seems to influence the aforementioned relations, as the significant activity of the *winter* SCAND at 6–10 years is timely synchronized with NAO's mode at 6–9 years (Figs.16e and 10a), while the combination of the two indices in opposite phases from the 1950 to the late-1970s enhances positive anomalies of precipitation along the studied area (e.g., Fig.5 in Comas-Bru and McDermott, 2013). On the other hand, no robust correlation was found between the SCAND index and SOI during the period 1950–2010. The strong coupling of Puglia's precipitation with SCAND in the sub-decadal scales is also imprinted in the high positive values of the correlation coefficient r_P (Table 3).

Similar to Puglia, the precipitation variability in the Greek Ionian region reveals two periods of strongly coherent variations with SCAND, but only limited common power (Fig.16b,e). Significant coherence, mostly prominent in the *monthly* series, was found at the 6–9 years band during the epoch of persistent positive SCAND phases (1950 to the late 1970s). The relative phases are then stabilized to $\delta\varphi \cong 120^\circ$ (Fig.16c) indicating a slightly *anti-phase* relation (also sensed by a low *negative* value of the monthly $r_P$coefficient in Table 3). From the late-1970s to the 2000s, as the SCAND activity is mostly modulated by the *winter* season variability, significant *in-phase* coherence becomes more pronounced in the *winter* series along the entire sub-decadal band. This fact also accounts for the puzzling sign reversion of the r_P global correlation coefficient between the RPC-2 series and SCAND, from a negative value

($r_P = -0.14$) regarding the monthly series to a positive value ($r_P = 0.23$) between the winter series.

4.2.5. Relations with EA-WR

The power distribution of the *winter* EA-WR index in the time-scale domain shows that since 1950 the EA-WR exhibits significant activity only at the 3–6 years band. Significant modes of precipitation along the studied area have been detected at 3–6 years (Table 2) but none of them was found to be concurrent with the EA-WR activity. Nevertheless, the *winter* RPC1 series reveals significant coherence with EA-WR at the 3–6 years band until the mid-1970s, and afterwards only at the short scales. This relation becomes more pronounced in the Taranto *winter* precipitation mode at 4.9 years. Much stronger significant *anti-phase* coherence with EA-WR over the 3–8 years band was found in case of the RPC2 series until the mid-1970s, particularly in the southern part of the region. This relation is also imprinted in the global linear correlation coefficient r_P as a relatively high anti-correlation value (Table 3). Regarding the studied area, the aforementioned picture is consistent with Ionita's (2014) results for the EA-WR impact on the precipitation over the Euro-Mediterranean sector.

4.2.6. Relations with QBO

Strong oscillatory modes of precipitation variability at 2.3–2.4 years were detected in many stations of the studied area, with the case of Leuca being the most characteristic (Figs.4a, 5a). Similar modes have been found in the precipitation field of many European and Mediterranean areas (Brázdil and Zolotokrylin, 1995; Lopez-Bustins et al., 2007; Karagiannidis et al., 2008 and references therein), as well as in air temperature, SST, and SLP (Johnstone, 2010). Their origin has been frequently associated with the stratospheric zonal wind quasi-biennial oscillation at 27–29 *months* (2.3–2.4 years) and with the effects of the downward propagating wave-train in the general circulation (Baldwin et al., 2001 and references therein; Lopez-Bustins et al., 2007; Johnstone, 2010). In this way, the stratospheric QBO variability affects the troposphere (Mohanakumar, 2008; Dall'Amico et al., 2010) which seems to possess a slightly different QB mode probably at 2.1–2.2 years, often referred as the *tropospheric biennial oscillation* or TBO (e.g., Zheng et al., 2008). However, the possibility for short-scale components such as the detected 2.3–2.4 years modes, to be a spectral aliasing artifact due to the implication of a harmonic functional basis in the underlying analysis has to be considered, as warned by Kirchner(2005). Nevertheless, the detected QB modes proved to be a robust feature of the precipitation variability in the studied area, as: (i) they were detected by SSA, where a non-harmonic data-adaptive functional basis is used, (ii) they were detected by all the other spectral analysis methods besides their different functional basis and methodologies, (iii) their characteristics remained practically invariant from the analysis of both the annual and monthly series. Hence, although spectral inflation can't be ruled out, we consider that the QB modes in the studied area have a natural origin.

In this framework, the relations of the RPC1,2 series with the adopted QBO index were searched at 2.3–2.4 years, with the exceptional case of Leuca being in focus. The *monthly* RPC1 series reveals significant coherence with QBO only during the 1990s, although significant common power was detected almost along the entire observational period (1921–2010). The relative phases exhibit transitions of about 180° during the different periods of enhanced coherence, with bounded oscillation in between, while $\delta\varphi_c$ reveals a multi-modal distribution. These facts do not indicate a simple cause-and-effect physical relation between QBO and RPC1. This estimation is further enhanced by the corresponding relation of Leuca's precipitation mode at 2.3 years with QBO where significant coherence was detected only during the 1970s (a low variance period for Leuca's QB mode) while no relation was found between the winter series in these scales (Fig.17a). On the contrary, significant and steady *in-phase* coherence prevails with SCAND at the 2–3 years band (particularly during the winter season),

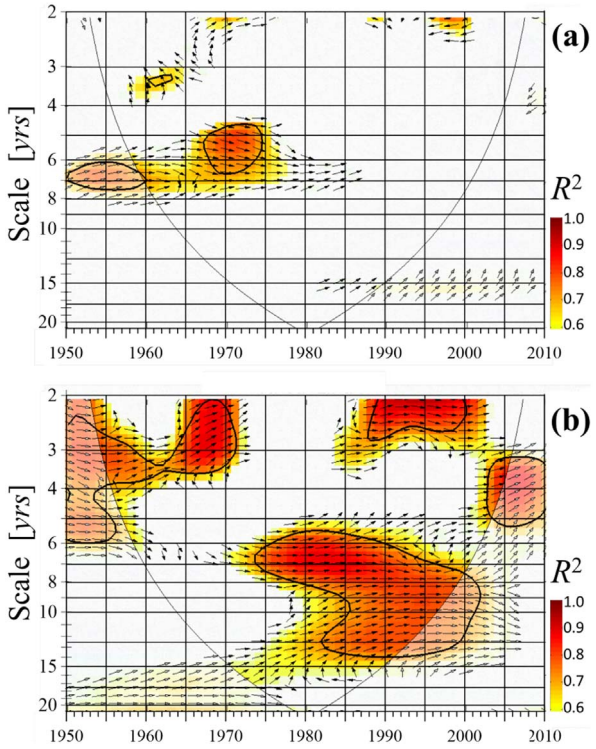

Fig. 17. Wavelet coherence of the *winter* precipitation in Leuca with QBO (a) and with SCAND (b). The relative phases $\delta\varphi$ are seen by the small arrows (according to the convention given in Fig.6).

whose evolution is compatible to the amplitude variability of Leuca's mode (Fig.17b). This fact verifies the estimation made earlier (in Section 4.2.4) that *the strong quasi-biennial precipitation variability in Leuca and the Taranto Gulf side of Puglia is mostly driven by* SCAND. Similar conclusions are drawn for the relation of the *monthly* RPC2 series with QBO in the Greek Ionian region.

5. Discussion and conclusions

A detailed exploration of the climatic precipitation variability along Puglia (Italy) and the Greek Ionian region during the last century is performed in this study. Three regions of precipitation variability were discerned along the studied area in respect to the underlying climatic dynamics: (i) the Adriatic side of Puglia, (ii) the Taranto Gulf side, and (iii) the Greek Ionian region, with the Otranto strait (represented in our sample by the Otranto and Corfu stations) being a transitional area. The observed precipitation variability in the adopted stations was found to be dominated by up to 3 significant modes, roughly accounting for 40–60% of the total variance (Table 2). The climatic dynamics of the studied area, as captured by the evolutionary characteristics of these precipitation modes and by their coupling with certain patterns of climatic variability, can be reviewed according to the different time-scales, as follows:

i) Relatively weak *multidecadal* ($s > 30$ years) modes were detected only in a few locations along the Adriatic side of Puglia and the Greek Ionian region. The exploration of their relations with SOI and NAO was by necessity restricted to the Greek Ionian region where long-scale modes ($s \cong 42$ years) of precipitation variability were found to be highly related with both ENSO and NAO. In particular, since the beginning of the 20th century significant *in-phase* coherence was detected with SOI and significant common power after the 1950s (Fig.9). At the same time (1950s) significant *anti-phase* coherence appeared with the *winter* NAO, which is consistent with the relation between the SOI and NAO indices at these scales.

Nevertheless, being close to the upper detectability limit of the applied methods ($s_M \cong 50$ years), these relations should be considered under the precaution of reduced credibility.

ii) Significant *bi-decadal* modes (at $s \cong 21$ years) were detected in the Adriatic side of Puglia and in Corfu area. They were found to be related with an enhanced bi-decadal SOI activity from the mid-1930s to the mid-1980s through significant *in-phase* coherence *and* common power. A limited relation also traced with a weak bi-decadal component of the *winter* NAO from the late 1930s to the late 1960s, which is upgraded in the Greek Ionian region to significant *anti-phase* coherence. However, the impact of this NAO component on the amplitude of the bi-decadal precipitation modes was rather limited in all cases, while no other significant relationship was detected with EA, SCAND, or EA-WR. Thus, the possible effects of the Atlantic Ocean SST intrinsic variability was further searched for as a potential modulator of the bi-decadal precipitation variations in the Adriatic side of Puglia, since the associated Atlantic Multidecadal Oscillation (or AMO) index exhibits strong modes at the multidecadal scales (Knight et al., 2006; Guan and Nigam, 2009; Deser et al., 2010). Apart from ENSO and possible anthropogenic forcing, a natural bi-decadal mode of the Atlantic Meridional Overturning Circulation (or AMOC) might be entangled in AMO variability, as anticipated by relevant models of the oceanic thermohaline circulation (Marshall et al., 2001; Tulloch and Marshall, 2012). We found that although the Atlantic ocean-atmosphere coupling is pronounced in the relation between the NAO HSt and AMO indices in both the decadal and sub-decadal scales, it fades in the longer scales. As a result, apart from significant common power from the early 1940s to the early 1970s, the Adriatic stations precipitation variability reveals only weak coherence with AMO at the bi-decadal scales. Although distinguishable, this relation with AMO is considerably weaker than with SOI. Hence, *it seems that among the examined patterns of climatic variability*, ENSO *prevails as the main agent of the bi-decadal precipitation variations in the Adriatic side of Puglia*. Nevertheless, as the corresponding bi-decadal variability in SOI is not significant, further search is needed for this conclusion to be verified.

iii) Powerful *decadal* and *quasi-decadal* modes (at 10–15.5 years) were detected along the studied area, except from the Adriatic side of Puglia and Corfu. The spatiotemporal diversity of the decadal precipitation variability proved to be much more complicated than in the longer scales. Possibly the most important characteristic of the detected decadal precipitation variability is located in its temporal synchronization with two major periods of ENSO exceptional activity during the 20th century (from 1900 to the mid-1920s, and from the early 1970s to the 2000s). During these periods, the decadal precipitation variability reveals characteristics of transient synchronization events with SOI, particularly in the southern Greek Ionian region where it exhibits significant *in-phase* coherence *and* common power with SOI from the 1890s to the mid-1920s (Fig.7a–d). This is also valid for the Taranto Gulf stations, where a remarkable response is detected to ENSO's decadal signals in terms of highly significant *anti-phase* coherence *and* common power from the early 1970s to the 2000s (Fig.7e–h). The precipitation response to ENSO's signals weakens in the Adriatic side, although significant *anti-phase* coherence is still sensed between the *winter* series. This relation, along with the effects of EA variability is suspected to sustain the strong decadal precipitation mode in Otranto after the late-1970s. The decadal *winter* precipitation variability (at the 8–12 years band) in the Taranto Gulf stations was additionally found to be related with the SCAND after the late 1970s, in terms of significant *in-phase* coupling. The relation with SCAND fades towards the Adriatic side of Puglia (where the EA influence at the bi-decadal scale predominates), with the characteristic decadal variability in *Otranto* possibly representing a transitional regime.

iv) Significant *sub-decadal* oscillatory modes were found in the Taranto Gulf side of Puglia (at 2–5 years) and in the southern Ionian region (at 5–9 years). The intense short scale precipitation variability in the Taranto Gulf side (prominent in Leuca area at 2.3 years) seems to be strongly modulated by SCAND through *in-phase* coupling and transient synchronization events. In the Greek Ionian region, SCAND also affects the *winter* short scale variability but less than in the Taranto Gulf area, while only limited effects are detected in the Adriatic side (similar to the regime found in the decadal scales). Because the SCAND activity has a strong influence on the Mediterranean cyclogenesis and on the southern circulation, its high impact on the Ionian Sea locations (which are freely exposed to sirocco-type southern circulation) becomes well understood. Additionally, the strong variance of the local precipitation to the short scales seems to be a direct result of SCAND inherent high frequency variability triggered by the transient eddies activity along the Atlantic storm track in combination with the prevailing Rossby-wave packet propagation (Bueh and Nakamura, 2007). The significant variability at 7–8 years in the Greek Ionian region is found to be synchronized with SOI sub-decadal activity from early 1900s to mid-1920s, and simultaneously with an enhanced *winter* NAO component at 6–9 years (Figs.6d, 10c). The *winter* precipitation modes at 7–8 years seem to be mostly excited during periods of NAO persistence in strong *positive* phases (where $\delta\varphi$ tends to 90°), while during the intervals of NAO persistency into negative or alternating phases, this mode fades and a weak *anti-phase* relation prevails. This peculiar behavior might be associated with the limited exposure of the Greek Ionian region to the enhanced northwestern circulation which is established under negative NAO phases [as it was also suggested by Coscarelli et al., 2013 for the observed weakening of the precipitation coupling with NAO, between the Tyrrhenian and the Ionian Sea sides of Calabria]. After the late 1980s, similar modes appeared in the winter precipitation of the Adriatic stations, which were found to be significantly related only with NAO.

Combined, the remarks made in (i)–(iv) show that *the precipitation variability along the Taranto Gulf and the southern Greek Ionian regions responds to* ENSO's *decadal signals* (*either directly or through transitive relations with regional patterns of climatic variability*) *and to* SCAND's *short scale forcing* (*through the effects of sirocco-type circulation*) *under important implications of* NAO *and* EA. *In the Adriatic coast of Puglia where the Bora-type circulation prevails, the SCAND effects fade and the greatest part of the local precipitation variability is spotted at the bi-decadal scales, while the decadal variability is temporarily affected by the EA during the winter*. Nevertheless, in the framework of the lowest order (1:1) uni-directional coupling assumption, the detected bi-decadal variability is not explained sufficiently by the activity of any particular climatic pattern, besides the indications of certain statistical relations with ENSO and AMO. The high response of Otranto's area to decadal precipitation signals possibly reflects a transitional state between the two aforementioned regimes.

v) An important aspect of the studied area response to global or regional scale climatic shifts is carried by the significant discontinuities detected in the precipitation variability of the Otranto strait region (in 1962 at Otranto and 1964 at Corfu), and particularly of the southern Greek Ionian region and Taranto in 1971–1972 (Fig.A1). *An abrupt decrease of the mean annual precipitation height followed these events*. Further discontinuities of a moderate intensity, but of an uncertain origin, are also spotted in 1933–1935 and 1947–1948 in southern Puglia. Regarding the 1962–1964 discontinuities, only some insufficient evidence was found relating them with the strong NAO multidecadal fluctuation (from the 1950s to the 2000s) and the relevant onset of the significant positive trend in NAO at the 1960s (Fig.10a). On the other hand, the discontinuities at the early 1970s occurred almost immediately after

the onset of ENSO's exceptional broad-band activity epoch (late 1960s) while they are detected only in stations where the relation with SOI was found to be strong enough (Taranto, Zakynthos, and Cephalonia). Hence, these events are suspected to be associated with the 1970s ENSO - Pacific climate shift that disturbed critical parts of the general circulation, the coupling with regional climatic patterns, and finally induced changes in many sub-regional systems (Allan, 2000; Hilmer and Jung, 2000; Enfield and Mestas-Nuñez, 2000; Rimbu et al., 2003; Walter and Graf, 2002; Knippertz et al., 2003). At the same time the strong multidecadal NAO fluctuation switched from negative (1950–1970) to positive (1970–2000) phases, while the SCAND persistence in positive phases came to an end. Hence, in the early 1970s the new ENSO regime, combined at the regional scale with the concurrent NAO-SCAND opposite phases, possibly triggered an abrupt reduction of the annual precipitation (up to 20%) in certain locations of Central Mediterranean, such as the Taranto Gulf and the Greek Ionian region. The aforementioned facts indicate that ENSO's *effects at the Ionian Sea area become significant in a non-linear way* (*hence, manifested when an activity threshold is overwhelmed*). The implications of ENSO, SCAND, and NAO in the timing and the modulation of these events, combined with the divergent precipitation response in the different modes and scales, seem to smear-out the effects of climatic shifts –such as the 1970s- in some locations and leave isolated detections of strong discontinuities in others.

Acknowledgements

The authors greatly acknowledge the valuable suggestions made by the associate editor Prof. S. Michaelides and by two unknown reviewers. The provision of precipitation data for the studied area from the Italian Ufficio Idrografico e Mareografico, and the Hellenic National Meteorological Service are also acknowledged, as well as the wavelet analysis MatLab codes by C.Torrence and G.Compo through http://paos.colorado.edu/research/wavelets/. Part of this work was supported by the European Community, Greece – Italy 2007–2013, Interreg IV DEMSNIISI project, MIS 902016 (Kalimeris et al., 2016).

Authors' contributions

All authors have made substantial contribution to the conception and design of the study, the drafting, the revision, and the artwork of the article, as well as to the physical interpretation of the results (Section 5). They also performed the extended search of relations between the observed precipitation variability and the main climatic patterns (in Section 4). Additionally, *E. Ranieri* and *D. Founda* contributed the data acquisition, preparation, and descriptive statistics, while *C. Norrant* and *A. Kalimeris* provided Rotated Principal Components Analysis and stations clustering. Finally, *A. Kalimeris* and *D. Founda* performed missing values estimation, homogenization, and the spectral decomposition analysis (Sections 3, 4, and the Appendices).

Appendix A. Missing values estimation and homogenization

Before missing values estimation, *data quality control* performed for the detection of possible outliers through *PRODIGE* in the framework of the *HOMER* homogenization method (Caussinus and Mestre, 2004). However, since the high spatial and temporal variability of precipitation increases the risk of false rejections of true local extremes (Domonkos, 2015), only the most abnormal monthly values filtered-out as possible outliers (most of them found at the southern Greek Ionian stations of Cephalonia and Zakynthos during 1910–12).

A.1. Missing values estimation

Two broad categories of missing values estimation procedures are generally considered for the analysis of climate time series: those applying *spatio-temporal interpolation* techniques and those incorporated within a *homogenization procedure*. Spatial interpolation techniques are based on various interrelation measures between the original time series or their differences (such as, correlation, coherence, and distance indices; Pigot, 2001; Schneider, 2001; Beckers and Rixen, 2003; Staudt et al., 2007; Vicente-Serrano et al., 2010). Missing values are ideally expected to be randomly distributed (Little and Rubin, 1987; Schafer, 1997) and synchronous data gaps between network stations to be absent. However, depending on the actual distribution of missing values, on the gaps length, and on the correlation strength of the examined series, spatial interpolation might be not a feasible option (as for example are the lengthy data gaps related with WW-II, which are synchronous in many stations and not randomly distributed). Under such circumstances, which are met in the precipitation series of the Greek Ionian region, *temporal interpolation* through advanced data adaptive algorithms might be the only gap-filling option. Nevertheless, since in this case spatial or temporal interpolation is applied before homogenization, biased missing values estimations might emerge (due to the existence of possible inhomogeneities in the original data) eventually to be corrected in the homogenization phase. Alternatively, missing values estimation can be performed as a part of the homogenization procedure. In this case, the possible brake-points are taken into account before gap filling and hence, an unbiased reconstitution of missing values is expected. However, in cases of *successive synchronous gaps* in neighborhood stations (like those existed in the series of the Greek Ionian region) the risk of false break detections and subsequent biased missing values estimation, increases. For example, in our preliminary computations through *HOMER*, artificial pairwise detections of break-points emerged at the times associated with the beginning or the end of the data gap periods in these stations, which subsequently affected the next stages of the procedure. Hence, temporal interpolation was applied here in case of the Greek Ionian stations and spatial interpolation in case of Puglia stations. In particular, in each station missing data filling realized *for each month separately* by using one of the following two techniques:

(i) A *correlation-weighted linear least square* (or *cwls*) computational scheme, or.
(ii) *Iterative Singular Spectrum Analysis* (hereafter i*SSA*).

The *first* procedure applied in well correlated stations without synchronous data gap periods (i.e., in the Italian stations) while the *second* procedure applied in the Greek Ionian stations. The applied *cwls* procedure reveals structural similarities to that provided by Staudt et al. (2007), since an estimation $\widehat{H}_{i,j}$ of a missing precipitation value $H_{i,j} \equiv H_i(t_j)$ in the i-station [$i = 1(1)n$] during the j-month [$j = 1(1)12$] is based on the observed values $H_{k,j}$ in each one of the rest $n - 1$ stations of the network [$k = 1(1)n$, $k \neq i$] through the equation:

$$\widehat{H}_i(t_j) \equiv \widehat{H}_{i,j} = \sum_{k=1}^{n} \left(r'_{ik,j} \cdot h_{ik,j}\right) \Big/ \sum_{k=1}^{n} r'_{ik,j}, \quad \text{with } k \neq i \tag{A.1}$$

In Eq. (A.1), $h_{ik,j}$ is the kth partial prediction of the missing value $H_{i,j}$, which is provided by the observed value $H_{k,j}$ in the k-station through linear

least squares regression:

$$h_{ik,j} = \beta_1 \cdot H_{k,j} + \beta_0,$$
$$k = 1(1)n,\ k \neq i,\ j = i(1)12 \tag{A.2}$$

Actually Eq. (A.2) *relates the precipitation height of the i-station during the j-month with the corresponding observed values at the best correlated k-stations*. In addition $r_{ik,j}^{'} = r_{ik,j}$ is set in Eq.(A.1) when the linear correlation coefficient $r_{ik,j}$ between the *i*th and *k*th stations is statistically significant at a prescribed level (typically 0.05) and $r_{ik,j}^{'} = 0$ otherwise, provided that there is at least one *k*-value ($k \neq i$) such that $r_{ik,j}^{'} \neq 0$ (that is, when observations from at least one significantly correlated station are available). Through the aforementioned procedure, any missing value of precipitation in the *i*-station during the *j*-month is estimated by appropriately weighting the observed values of the significantly correlated stations. This scheme is also applicable through sliding time-windows when the temporal correlation variations of the target and the neighborhood stations should be taken into account.

On the other hand, the i*SSA* algorithm described by Kondrashov and Ghil (2006) applied in case of missing values estimation in the Greek Ionian stations. In this procedure, missing values are actually estimated through a continuous flow of information related to the variability modes of precipitation (quantified by the temporal empirical orthogonal functions, or EOFs, of the studied series lag-covariance matrix) towards the data gap intervals. A double iterative scheme is used for this goal in combination with a set of cross-validation experiments according to an *artificial missing point random seed technique*. The fraction f_{rs} of randomly selected observed data (which were flagged as artificial missing points) that was adopted in our computations was between 0.05 and 0.15, while the number K_* of the retained modes in the precipitation series *of each month separately* were ranging between $K_* = 3$ and $K_* = 20$, depending on the data gap length and the overall variability of the series.

A.2. Homogenization

Relative homogenization of the adopted monthly precipitation series performed through the *CLIMATOL* (Guijarro, 2011, 2013), *HOMER* (Mestre et al., 2013; see also Caussinus and Mestre, 2004; Picard et al., 2011; Domonkos, 2011), and $ACMANT_2$ (Domonkos, 2015) methods, whose efficiency has been analyzed by Venema et al. (2012), and Domonkos (2015). In case of *HOMER* a maximum number of three iterative correction steps were applied under the interactive mode, both for the original and the data-filled series. The detected braking points are summarized in Table A.1, while the corrected series for two representative stations are illustrated in Fig. A1. *Absolute homogeneity* tests also applied in the *annual* series through the Pettitt, Buishand, Standard Normal Homogeneity or *SNHT*, and von Neumann algorithms (Alexandersson, 1986; Buishand, 1982; Pettitt, 1979; Von Neumann, 1941). Regarding the Italian stations of Puglia, only moderate magnitude breaking-points found in *Leuca*, *Otranto*, and *Taranto*. In particular, two braking-points detected at 1933–35 and 1947–48 in *Leuca* by all methods (but only through some pairwise comparisons in *HOMER*). Breaking-points also jointly detected by *HOMER* and *CLIMATOL* in *Taranto* at 1971–72 (at the same time with the strong discontinuities found in the southern Greek Ionian stations) and at 1947–48 only by $ACMANT_2$ (Fig.A1a). Finally, another discontinuity detected by $ACMANT_2$ in *Otranto* at 1964. The artificial or climatic origin of these breaking points can't be safely assessed as no metadata were available for these stations in the dates of interest.

Available metadata in the Greek Ionian stations show a history of small relocations associated with limited environmental and topographic changes. The most important relocations realized at 1949 in Corfu, at 1984 in Cephalonia, and at 1982 in Zakynthos, when these stations moved from the town outskirts to the nearby airports (in distances 3–7 km). Further minor relocations, associated with small height changes (of the order of 10 m) are known to be happened at 1911, 1912, and 1926 in Corfu station (Kotinis-Zambakas et al., 1996), and at 1918 in Zakynthos. Finally, changes in observational practices and/or equipment are highly suspected to be happened between 1931 and 33 and around 1955 in these stations, but they are not well documented. Regarding the possible origin (*artificial* or *climatic*) of the detected breaking points we only examined those events that were jointly detected by at least two relative homogenization methods. As it is seen in Table A.1 there is only *one strong discontinuity* that was jointly detected by all methods at 1971 in Cephalonia (also detected as statistically significant by all absolute methods). Similar discontinuities also detected at the neighborhood Zakynthos station in the 1971–73 interval (Fig. A1b), and Corfu at 1962 (none of them verified by $ACMANT_2$). Some further joint detections around 1925–26 and 1933 in Corfu and Cephalonia are possibly related with relocations or technical changes in these stations. However, none of the 1971–73 or 1962 discontinuities are associated with periods of missing values, known relocations, changes of observing practices, strong or abrupt environment changes. Hence, a climatic origin is suspected for these discontinuities, as discussed in Section 5.

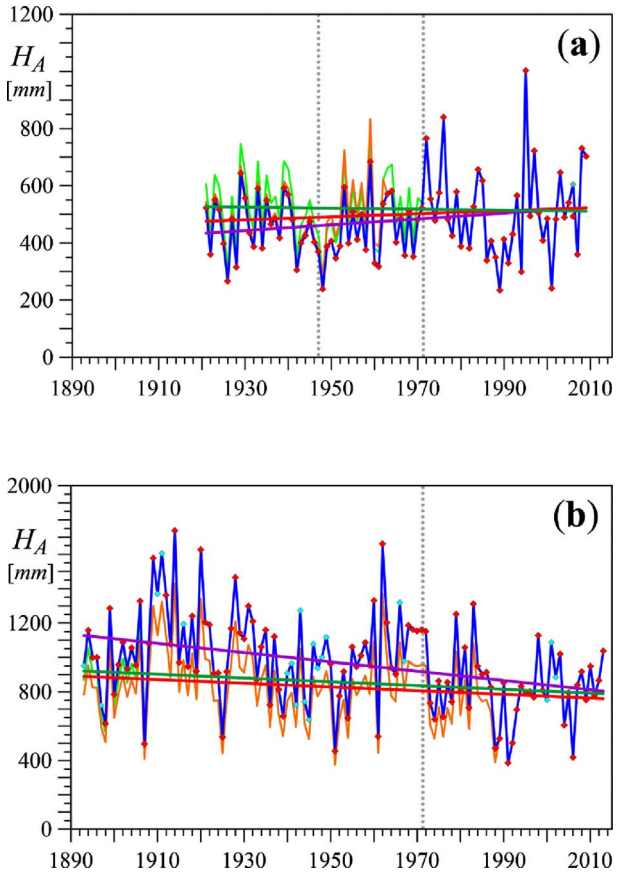

Fig. A1. The observed (blue line), the *ACMANT*$_2$ (orange line) and the *HOMER* (green line) corrected annual precipitation variability in Taranto (a) and Zakynthos (b). The corresponding linear trends are shown by the purple, red, and green lines respectively for the observed, the *ACMANT*$_2$, and the *HOMER* series. The vertical dashed lines indicate the position of significant discontinuities (see also Table A.1). (For interpretation of the references to colour in this figure legend, the reader is referred to the web version of this article.)

Table A.1

Dates of break points detected in the *monthly* precipitation series of each station (for clarity, detections separated by less than 4 years are listed in the same row). Bolded underlined values indicate discontinuities jointly found by all methods, while those detected by *CLIMATOL* and at least one of *ACMANT*$_2$ or *HOMER* are indicated by underlined italics. Break points associated with known relocations are marked by an asterisk. Finally, discontinuities that were detected in the *annual* precipitation series by the absolute homogeneity tests are also listed in the last row (significant detections are underlined).

	Bari	Brindisi	Taranto	Otranto	Gallipoli	Leuca	Corfu	Cephalonia	Zakynthos	Methoni
Observations period	1938–2010	1921–2010	1921–2010	1921–2010	1921–2010	1921–2010	1887–2014	1893–2014	1893–2014	1956–2012
ACMANT$_2$ detections							1926*	1929, 1933*		
						1935				
			1948			***1948***	1951			
			1963							
								1971		
									1989	
CLIMATOL detections								1906	***1909***, ***1913***	
							1921	1917		
						1933	1933*			
		1951		1949, 1951	1951	***1948***				
		1959		***1964***	1961		***1963***		1962	
		1972	***1972***/ 76–77					**1972**	***1973***	
				1991	1990					
			1995, 1997		1996					

HOMER detections							1909		***1909***, ***1912***	
							1925*			
								1929, 1933*		
				1964			***1962***			
			1971					***1971***	***1971***	
Absolute homogeneity detections	1983	1950	1947	*1964*	1960/1990	1947–50	1973/ ***1964***	***1972***	***1972***	1963

Appendix B. Coherence and synchronization measures

The instantaneous amplitudes $\alpha_k(t_j)$ and phases $\varphi_k(t_j)$ of each reconstructed spectral component with rank k, are provided in spectral analysis in reference to a nominal frequency f_k over the entire observational period. However, in wavelet analysis each mode can be localized in the time-frequency (or equivalently, the time-scale) domain by the distribution of its instantaneous power $S(t_j)$ over an interval of scales $[s_\ell, s_u] = \Delta_S$; the time scale s corresponding to the Morlet wavelet with $\omega_0 = 6$ almost coincides with the Fourier time wavelength or period T, since $T = 4\pi \cdot s/(\omega_0 + \sqrt{2 + \omega_0^2}) \cong 1.033 \cdot s$ (e.g., Torrence and Compo, 1998). Then, the scale $s_k(t_j)$ corresponding to the local maximum of $S(t_j)$ over Δ_S can be used as a measure of this mode frequency $f(t_j)$ at the time t_j [$j = 1(1)n$]. The frequency f -or scale s - evolution of a mode can be estimated in this way by tracing the local maximum value of $S(t_j)$ within an appropriate scales interval Δ_S. Hence, the relation of the frequencies $f_{x,k}(t_j)$, $f_{y,l}(t_j)$ of two modes with ranks k, l in the time series $x(t_j)$, $y(t_j)$ (corresponding to the driver oscillator and the coupled regional system, respectively) can be similarly explored in the time-scale domain along with the covariance or a correlation measure of their amplitudes $\alpha_{x,k}$, $\alpha_{y,l}$ and with their *phase difference* or *relative phase* $\delta\varphi_{kl}(t_j) = \varphi_{x,k}(t_j) - \varphi_{y,l}(t_j)$. Provided that a physical coupling of the regional climatic system is known with a climatic oscillator, an *f*-type synchronization can be inferred when $f_{x,k}(t_j) \cong f_{y,l}(t_j)$ over a time interval, and an *fp*-type when a nearly *steady or bounded phase difference* $\delta\varphi$ is additionally observed. Further enhancement of coupling will enforce coherent variations in the amplitudes α_x, α_y and hence, strong and statistically significant covariance or correlation will be implied in addition to the aforementioned relations. When a physical coupling is not a priori known, its presence can be inferred by the detection of a *unimodal* frequency distribution of the *cyclic relative phases* $\delta\varphi_c$ (Rosenblum et al., 2001; Osipov et al., 2003). The latter quantity is introduced in order to eliminate the addition of complete cycles in the time evolving phase difference values, by the equation:

$$\delta\varphi_c = \delta\varphi \mod(2\pi) \tag{B.1}$$

However, in the presence of strong stochastic or irregular variations, the distribution of $\delta\varphi_c$ might take the form of a dual- or multi-modal distribution.

A localized measure of covariance between $x(t_j)$ and $y(t_j)$ is their common power which is quantified in the time-scale domain by the Cross-Wavelet Transform, defined for each time t_j, $j = 1(1)n$, and scale s by (e.g., Grinsted et al., 2004):

$$W_{t_j}^{xy}(s) = W_{t_j}^{x}(s) \cdot W_{t_j}^{y*}(s) \tag{B.2}$$

where $W_{t_j}^{x}(s)$, $W_{t_j}^{y}(s)$ are the wavelet transformations of the x and y series respectively, and $W_{t_j}^{y*}(s)$ the complex conjugate of $W_{t_j}^{y}(s)$. Since the Cross-Wavelet Transform $W_{t_j}^{xy}(s)$ indicates the scales where *locally enhanced* spectral power -then amplitudes as well- commonly prevails in both series, it can be also considered as an indirect index of the amplitudes relation between $x(t_j)$, $y(t_j)$. Following Torrence and Compo (1998), the upper useful scale s_M adopted in wavelet transformation computational algorithm was equal to:

$$s_M = 1.03 \cdot (n \cdot \delta t/3) \tag{B.3}$$

(δt being the sampling interval). To eliminate artificial power distribution caused by the fact that long period wavelets are not completely localized in time as their extent become comparable to the time series width, the cone of interest (COI) feature is used as the conical area in the time-scale domain where the wavelet power caused by a discontinuity at the edge has dropped to e^{-2} of the edge value (e.g., Grinsted et al., 2004). Then, for each moment t_j, an upper useful scale $s_{coi}(t_j)$ exists (with $s_{coi} \le s_M$) such that, higher credibility to be given in spectral features with scales $s \le s_{coi}$ (located at the interior of COI). In subsequence, the relative phase $\delta\phi_{t_j}(s)$ between $x(t_j)$, $y(t_j)$ at a scale $s \le s_M$ can be implied by the complex argument $\arg(W^{xy})$ of $W_{t_j}^{xy}(s)$, according to the equation:

$$\delta\varphi_{t_j}(s) = \arctan\left[\frac{\mathcal{I}m\{\langle s^{-1} \cdot W_{t_j}^{xy}(s)\rangle\}}{\mathcal{R}e\{\langle s^{-1} \cdot W_{t_j}^{xy}(s)\rangle\}}\right] \tag{B.4}$$

where $\mathcal{R}e\{\}$ and $\mathcal{I}m\{\}$ are respectively the real and imaginary parts of $W_{t_j}^{xy}(s)$, while $\langle\ \rangle$ represents a smoothing operator over time and scale, analytically described by Torrence and Compo (1998), and by Grinsted et al. (2004). Values of $\delta\varphi$ according to Eq. (B.4) are in close agreement to those obtained by the non-parametric computation through the Hilbert transformation (Quiroga et al., 2002; Kreuz et al., 2007). Finally, a coherence measure $R_{t_j}^2(s)$ between $x(t_j)$, $y(t_j)$ at the time t_j and scale s can be defined by the equation (Torrence and Webster, 1999):

$$R_{t_j}^2(s) = \frac{|\ \langle s^{-1} \cdot W_{t_j}^{xy}(s)\rangle\ |^2}{\langle s^{-1} \cdot |\ W_{t_j}^{x}(s)\ |^2\rangle \cdot \langle s^{-1} \cdot |\ W_{t_j}^{y}(s)\ |^2\rangle} \tag{B.5}$$

where the operator $|\ \ |^2$ represents wavelet power (for simplicity $R_{t_j}^2(s)$ will be referred as R^2). Statistical significance of R^2 values can be implied by Monte-Carlo Continuous Wavelet Transform of $x(t_j)$, $y(t_j)$, and then depicted in the time-scale domain together with the relative phase $\delta\varphi$. In Eq. (B.5), wavelet coherence is defined in analogy with the *global* linear correlation coefficient r, but since it is based on the wavelet transform of the

studied time series, R^2 is *localized* in the time-scale domain. Hence, wavelet coherence is able to detect significant correlations in certain time-scales and epochs, which might be overestimated or even ignored by a global linear correlation coefficient.

References

Alexandersson, H., 1986. A homogeneity test applied to precipitation data. J. Clim. 6, 661–675.

Allan, R.J., 2000. ENSO and climatic variability in the past 150 years. In: Diaz, H.F., Markgraf, V. (Eds.), El-Niño and the Southern Oscillation – Multiscale Variability and Global and Regional Impacts. Cambridge University Press, pp. 3–55.

Allan, R.J., D'Arrigo, R.D., 1999. Persistent ENSO sequences: how unusual was the 1990–1995 El-Niño? The Holocene 9, 101–118.

Allen, M.R., Smith, L.A., 1996. Monte Carlo SSA: detecting irregular oscillations in the presence of coloured noise. J. Clim. 9, 3373–3404.

Alley, R.B., Anandakrishnan, S., Jung, P., 2001. Stochastic resonance in the North Atlantic. Paleoceanography 16 (2), 190–198.

Alpert, P., Baldi, M., Ilani, R., Krichak, S., Price, C., Rodó, X., Saaroni, H., Ziv, B., Kischa, P., Barkan, J., Mariotti, A., Xoplaki, E., 2006. Relations between climate variability in the Mediterranean region and the Tropics: ENSO, South Asian and African Monsoons, Hurricanes and Saharan Dust. In: Lionello, P., Malanotte-Rizzoli, P., Boscolo, R. (Eds.), The Mediterranean Climate: An Overview of the Main Characteristics and Issues. Elsevier, pp. 149–177.

Arnone, E., Pumo, D., Viola, F., Noto, L.V., La Loggia, G., 2013. Rainfall statistics changes in Sicily. Hydrol. Earth Syst. Sci. 17, 2449–2458.

Baldwin, M.P., Gray, L.J., Dunkerton, T.J., Hamilton, K., Haynes, P.H., Randel, W.J., Holton, J.R., Alexander, M.J., Hirota, I., Horinouchi, T., Jones, D.B.A., Kinnersley, J.S., Marquardt, C., Sato, K., Takahashi, M., 2001. The quasi-biennial oscillation. Rev. Geophys. 39, 179–229.

Barnston, A.G., Livezey, R.E., 1987. Classification, seasonality and persistence of low-frequency atmospheric circulation patterns. Mon. Weather Rev. 115, 1083–1126.

Bartholy, J., Pongrácz, R., Pattantyús-Ábrahám, M., 2009. Analyzing the genesis, intensity, and tracks of western Mediterranean cyclones. Theor. Appl. Climatol. 96, 133–144.

Beckers, J., Rixen, M., 2003. EOF calculations and data filling from incomplete oceanographic data sets. J. Atmos. Ocean. Technol. 20, 1839–1856.

Benzi, R., Parisi, G., Sutera, A., Vulpiani, A., 1982. Stochastic resonance in climate change. Tellus 34, 10–16.

Blackman, R.B., Tukey, J.W., 1958. The Measurement of Power Spectra From the Point of View of Communication Engineering. Dover, Mineola, NY.

Bolle, H.-J., 2003. Climate, climate variability, and impacts in the Mediterranean area: an overview. In: Bolle, H.-J. (Ed.), Mediterranean Climate – Variability and Trends. Springer-Verlag, pp. 5–86 (2003).

Borzelli, G.L.E., Gačić, M., Cardin, V., Civitarese, G., 2009. Eastern Mediterranean Transient and reversal of the Ionian Sea circulation. Geophys. Res. Lett. 36, L15108. http://dx.doi.org/10.1029/2009GL039261.

van den Boss, A., 1971. Alternative interpretation of maximum entropy spectral analysis. IEEE Trans. Inf. Theory 17, 493–494.

Brázdil, R., Zolotokrylin, A.N., 1995. The QBO signal in monthly precipitation fields over Europe. Theor. Appl. Climatol. 51, 3–12.

Brönnimann, S., 2007. Impact of El Niño-Southern oscillation on European climate. Rev. Geophys. 45, RG3003. http://dx.doi.org/10.1029/2006RG000199.

Brönnimann, S., Xoplaki, E., Casty, C., Pauling, A., Luterbacher, J., 2007. ENSO influence on Europe during the last centuries. Clim. Dyn. 28, 181–197.

Bueh, C., Nakamura, H., 2007. Scandinavian pattern and its climatic impact. Q. J. R. Meteorol. Soc. 133, 2117–2131.

Buishand, T.A., 1982. Some methods for testing the homogeneity of rainfall records. J. Hydrol. 58, 11–27.

Burg, J.P., 1967. Maximum entropy spectral analysis. In: Childers, D.G. (Ed.), 37th Annual International Meeting of the Society of Exploration Geophysicists, Oklahoma City, Okla. Modern Spectrum Analysis IEEE Press, Piscataway, N.J., pp. 42–48 (1978).

Buttafuoco, G., Caloiero, T., Coscarelli, R., 2011. Spatial and temporal patterns of the mean annual precipitation at decadal time scale in southern Italy (Calabria region). Theor. Appl. Climatol. http://dx.doi.org/10.1007/s00704-011-0398-8.

Caloiero, T., Coscarelli, R., Ferrari, E., Mancini, M., 2011. Trend detection of annual and seasonal rainfall in Calabria (Southern Italy). Int. J. Climatol. 31, 44–56.

Caussinus, H., Mestre, O., 2004. Detection and correction of artificial shifts in climate series. J. R. Stat. Soc. Ser. C 53, 405–425.

Cobb, K.M., Charles, C.D., Edwards, R.L., Cheng, H., Kastner, M., 2003. El Niño/Southern Oscillation and tropical Pacific climate during the last millennium. Nature 424, 271–276.

Comas-Bru, L., McDermott, F., 2013. Impacts of the EA and SCA patterns on the European twentieth century NAO-winter climate relationship. Q. J. R. Meteorol. Soc. 140 (679), 354–679.

Comin, A.N., Miglietta, M.M., Rizza, U., Acevedo, O.C., Degrazia, G.A., 2015. Investigation of sea-breeze convergence in Salento Peninsula (southeastern Italy). Atmos. Res. 160, 68–79.

Coscarelli, R., Caloiero, T., 2012. Analysis of daily and monthly rainfall concentration in Southern Italy (Calabria region). J. Hydrol. 416–417, 145–156.

Coscarelli, R., Caloiero, T., Lo Feudo, T., 2013. Relationship between winter rainfall amount and teleconnection patterns in Southern Italy. Eur. Water 43, 13–21.

Crucifix, M., 2012. Oscillators and relaxation phenomena in Pleistocene climate theory. Phil. Trans. R. Soc. A 370, 1140–1165.

Da Costa, E.D., Colin De Verdiere, A., 2002. The 7.7-year North Atlantic oscillation. Q. J. R. Meteorol. Soc. 128, 797–817.

Dall'Amico, M., Stott, P.A., Scaife, A.A., Gray, L.J., Rosenlof, K.H., Karpechko, A.Y., 2010. Impact of stratospheric variability on tropospheric climate change. Clim. Dyn. 34, 399–417.

De Luis, M., Čufar, K., Saz, M.A., Longares, L.A., Ceglar, A., Kajfež-Bogataj, L., 2013. Trends in seasonal precipitation and temperature in Slovenia during 1951–2007. Reg. Environ. Chang. http://dx.doi.org/10.1007/s10113-012-0365-7.

Deser, C., Alexander, M.A., Xie, S.-P., Phillips, A.S., 2010. Sea surface temperature variability: patterns and mechanisms. Annu. Rev. Mar. Sci. 2, 115–143.

Domonkos, P., 2011. Adapted Caussinus-Mestre Algorithm for Networks of Temperature series (ACMANT). Int. J. Geosci. 2, 293–309.

Domonkos, P., 2015. Homogenization of precipitation time series with ACMANT. Theor. Appl. Climatol. 122, 303–314.

Elsner, J.B., Tsonis, A.A., 1996. Singular Spectrum Analysis: A New Tool in Time Series Analysis. Plenum Presspp. 161 (ISBN 0-306-45472-6).

Enfield, D., Mestas-Nuñez, A.M., 2000. Global modes of ENSO and non-ENSO sea surface temperature variability and their associations with climate. In: Diaz, H.F., Markgraf, V. (Eds.), El-Niño and the Southern Oscillation – Multiscale Variability and Global and Regional Impacts. Cambridge University Press, pp. 89–112.

Federico, S., Avolio, E., Pasqualoni, L., Bellecci, C., 2008. Atmospheric patterns for heavy rain events in Calabria. Nat. Hazards Earth Syst. Sci. 8, 1173–1186.

Federico, S., Pasqualoni, L., Avolio, E., Bellecci, C., 2010. Calabria daily rainfall from 1970 to 2006. Nat. Hazards Earth Syst. Sci. 10, 717–722 (Brief communication).

Feliks, Y., Ghil, M., Robertson, A., 2010. Oscillatory climate modes in the Eastern Mediterranean and their synchronization with the North Atlantic Oscillation. J. Clim. 23, 4060–4079.

Folland, C.K., Renwick, J.A., Salinger, M.J., Mullan, A.B., 2002. Relative influences of the Interdecadal Pacific Oscillation and ENSO on the South Pacific Convergence Zone. Geophys. Res. Lett. 29 (13), 1643. http://dx.doi.org/10.1029/2001GL014201.

Foufoula-Georgiou, E., Kumar, P., 1995. Wavelets in Geophysics. 373 Academic Press.

Fraedrich, K., Muller, K., 1992. Climate anomalies in Europe associated with ENSO extremes. Int. J. Climatol. 12, 25–31.

Gačić, M., Civitarese, G., Borzelli, E., Kovačević, G.L., Poulain, V., Theocharis, P.-M., Menna, M., Catucci, A., Zarokanellos, N., 2011. On the relationship between the decadal oscillations of the Northern Ionian Sea and the salinity distributions in the Eastern Mediterranean. J. Geophys. Res. 116, C12002. http://dx.doi.org/10.1029/2011JC007280.

Gačić, M., Schroeder, K., Civitarese, G., Vetrano, A., Eusebi Borzelli, G.L., 2012. On the relationship among the Adriatic–Ionian Bimodal Oscillating System (BiOS), the Eastern Mediterranean salinity variations and the Western Mediterranean thermohaline cell. Ocean Sci. Discuss. 9, 2561–2580.

Gámiz-Fortis, S.R., Pozo-Vázques, D., Esteban-Parra, M.J., Castro-Díez, Y., 2002. Spectral characteristics and predictability of the NAO assessed through singular spectral analysis. J. Geophys. Res. 107, 4685–4700.

Gershunov, A., Barnett, T.P., 1998. Interdecadal modulation of ENSO teleconnections. Bull. Am. Meteorol. Soc. 79, 2715–2725.

Ghil, M., Allen, M.R., Dettinger, M.D., Ide, K., Kondrashov, D., Mann, M.E., Robertson, A.W., Saunders, A., Tian, Y., Varadi, F., Yiou, P., 2002. Advanced spectral methods for climatic time series. Rev. Geophys. 40, 1–41.

Grinsted, A., Moore, J.C., Sevrejeva, S., 2004. Application of the cross wavelet transform and wavelet coherence to geophysical time series. Nonlinear Process. Geophys. 11, 561–566.

Gualdi, S., Somot, S., May, W., Castellari, S., Déqué, M., Adani, M., Artale, V., Bellucci, A., Breitgand, A.W., Carillo, A., Cornes, R., Dell'Aquila, A., Dubois, C., Efthymiadis, D., Elizalde, A., Gimeno, L., Goodess, C.M., Harzallah, A., Krichak, S.O., Kuglitsch, F.G., Leckebusch, G.C., L'Heveder, B., Li, L., Lionello, P., Luterbacher, J., Mariotti, A., Navarra, A., Nieto, R., Nissen, K.M., Oddo, P., Ruti, P., Sanna, A., Sannino, G., Scoccimarro, E., Sevault, F., Struglia, M.V., Toreti, A., Ulbrich, U., Xoplaki, E., 2013. Future climate projections. In: Navarra, A., Tubiana, L. (Eds.), Regional Assessment of Climate Change in the Mediterranean, vol. 1. Springer, Dordrecht, pp. 53–118.

Guan, B., Nigam, S., 2009. Analysis of Atlantic SST variability factoring inter-basin links and the secular trend: clarified structure of the Atlantic Multidecadal Oscillation. J. Clim. 22, 4228–4240.

Guijarro, J.A., 2011. User's guide to CLIMATOL. http://www.meteobal.com/climatol/climatol-guide.pdf.

Guijarro, J.A., 2013. Climatological series shift test comparison on running windows. Időjárás 117, 35–45.

Hilmer, M., Jung, T., 2000. Evidence for a recent change in the link between the North Atlantic Oscillation and Arctic sea ice export. Geophys. Res. Lett. 27, 989–992.

Hoerling, M.P., Kumar, A., 2000. Understanding and predicting extratropical teleconnections related to ENSO. In: Diaz, H.F., Markgraf, V. (Eds.), El-Niño and the Southern Oscillation – Multiscale Variability and Global and Regional Impacts. Cambridge University Press, pp. 57–88.

Homar, V., Jansà, A., Campins, J., Genovs, A., Ramis, C., 2007. Towards a systematic climatology of sensitivities of Mediterranean high impact weather: a contribution based on intense cyclones. Nat. Hazards Earth Syst. Sci. 7, 445–454.

Horvath, K., Lin, Y., Ivančan-Picek, B., 2008. Classification of cyclone tracks over the Apennines and the Adriatic Sea. Mon. Weather Rev. 136, 2210–2227.

Huang, J.-P., Higushi, K., Shabbar, A., 1998. The relationship between the North Atlantic

Oscillation and El Niño-Southern Oscillation. Geophys. Res. Lett. 25, 2701–2719.
Huffman, G.J., Adler, R.F., Bolvin, D.T., Gu, G., Nelkin, E.J., Bowman, K.P., Hong, Y., Stocker, E.F., Wolff, 2007. The TRMM Multi–satellite Precipitation Analysis: quasi–global, multi–year, combined–sensor precipitation estimates at fine scale. J. Hydrometeorol. 8, 38–55.
Hurrell, J., National Center for Atmospheric Research Staff, 2016. The Climate Data Guide: Hurrell North Atlantic Oscillation (NAO) Index (station-based). Retrieved from. https://climatedataguide.ucar.edu/climate-data/hurrell-north-atlantic-oscillation-nao-index-station-based.
Hurrell, J.W., Kushnir, Y., Ottersen, G., Visbeck, M., 2003. An overview of the North Atlantic Oscillation. In: Hurrell, J.W., Kushnir, Y., Ottersen, G., Visbeck, M. (Eds.), The North Atlantic Oscillation: Climatic Significance and Environmental Impact. Geophysical Monograph 134 American Geophysical Union, pp. 1–35.
Ineson, S., Scaife, A.A., 2009. The role of stratosphere in the European climate response to El Niño. Nat. Geosci. 2, 32–36.
Ionita, M., 2014. The impact of the East Atlantic/Western Russia pattern on the hydroclimatology of Europe from mid-winter to late spring. Climate 2, 296–309.
Ivančan-Picek, B., Horvath, K., Strelec Mahović, N., Gajić-Čapka, M., 2014. Forcing mechanisms of a heavy precipitation event in the southeastern Adriatic area. Nat. Hazards 72, 1231–1252.
Johnstone, J.A., 2010. A quasi-biennial signal in western US hydroclimate and its global teleconnections. Clim. Dyn. http://dx.doi.org/10.1007/s00382-010-0755-9.
Kaiser, H.F., 1958. The varimax criterion for analytic rotation in factor analysis. Psychometrika 23, 187–200.
Kalimeris, A., Founda, D., Giannakopoulos, C., Pierros, F., 2012. Long term precipitation variability in the Ionian Islands (Central Mediterranean): climatic signal analysis and future projections. Theor. Appl. Climatol. 109, 51–72.
Kalimeris, A., Kolios, S., Halvatzaras, D., Posa, D., DeIaco, S., Palma, M., Skordilis, C., Myrsilides, M., 2016. The Ionian-Puglia network of meteorological-environmental stations. I. Geophysical environment and technical description. Odysseus 7, 1–45.
Karagiannidis, F., Bloutsos, A.A., Maheras, P., Sachsamanoglou, Ch., 2008. Some statistical characteristics of precipitation in Europe. Theor. Appl. Climatol. 91, 193–204.
Kirchner, J.W., 2005. Aliasing in $1/f^{\alpha}$ noise spectra: origins, consequences, and remedies. Phys. Rev. E 71, 066110-1–066110-16.
Knight, J.R., Folland, C.K., Scaife, A.A., 2006. Climate impacts of the Atlantic Multidecadal Oscillation. Geophys. Res. Lett. 33, L17706.
Knippertz, P., Ulbrich, U., Marques, F., Corte-Real, J., 2003. Decadal changes in the link between El-Niño and spring North Atlantic oscillation and European-North African rainfall. Int. J. Climatol. 23, 1293–1311.
Kolios, S., Kalimeris, A., 2016. Annual and monthly precipitation variability in the Ionian Islands using 16-year TRMM data. In: Karacostas, T., Bais, A., Nastos, P. (Eds.), Perspectives on Atmospheric Sciences. Springer Atmospheric Sciences Springer.
Kondrashov, D., Ghil, M., 2006. Spatio-temporal filling of missing points in geophysical data sets. Nonlinear Process. Geophys. 13, 151–159.
Kotinis-Zambakas, S.J., Repapis, C.C., Philandras, C.M., Nastos, PTh, 1996. Compilation of the existing meteorological observations of the town of Kerkyra (1809–1990), no II: precipitation. Publ. Acad. Athens 15, 1–46 (in Greek).
Kreuz, T., Mormann, F., Andrzejak, R.G., Kraskov, A., Lehnertz, K., Grassberger, P., 2007. Measuring synchronization in coupled model systems: a comparison of different approaches. Phys. D 225, 29–42.
Krichak, S.O., Alpert, P., 2005. Decadal trends in the East Atlantic–West Russia pattern and Mediterranean precipitation. Int. J. Climatol. 25, 183–192.
Krichak, S.O., Kishcha, P., Alpert, P., 2002. Decadal trends of main Eurasian oscillations and the Eastern Mediterranean precipitation. Theor. Appl. Climatol. 72, 209–220.
Lau, N.-C., Nath, M.J., 2001. Impact of ENSO on SST variability in the North Pacific and North Atlantic: seasonal dependence and role of extratropical sea-air coupling. J. Clim. 14, 2846–2866.
Lionello, P., Giorgi, F., 2007. Winter precipitation and cyclones in the Mediterranean region: future climate scenarios in a regional simulation. Adv. Geosci. 12, 153–158.
Little, R.J.A., Rubin, D.B., 1987. Statistical Analysis With Missing Data. John Wiley and Sons, New York.
Lopez-Bustins, J.-A., Esteban, P., Labitzke, K., Langematz, U., 2007. The role of the stratosphere in Iberian Peninsula rainfall: a preliminary approach in February. J. Atmos. Sol. Terr. Phys. 69, 1471–1484.
Luterbacher, J., Xoplaki, E., 2003. 500-year winter temperature and precipitation variability over the Mediterranean area and its connection to the large-scale atmospheric circulation. In: Bolle, H.-J. (Ed.), Mediterranean Climate – Variability and Trends. Springer-Verlag, pp. 133–153 (2003).
Malanotte-Rizzoli, P., Manca, B.B., Ribera D'Alcalá, M., Theocharis, A., Bergamasco, A., Bregant, D., Budillon, G., Civitarese, G., Georgopoulos, D., Michelato, A., Sansone, E., Scarazzato, P., Souvermezoglou, E., 1997. A synthesis of the Ionian Sea hydrography, circulation and water mass pathways during POEM-phase I. Prog. Oceanogr. 39, 153–204.
Mangia, C., Martano, P., Miglietta, M.M., Morabito, A., Tanzarella, A., 2004. Modelling local circulations over the Salento Peninsula. Meteorol. Appl. 11, 231–244.
Mann, M.E., Bradley, R.S., 2000. Long-term variability in the El-Niño/Southern Oscillation and associated teleconnections. In: Diaz, H.F., Markgraf, V. (Eds.), El-Niño and the Southern Oscillation – Multiscale Variability and Global and Regional Impacts. Cambridge University Press, pp. 357–412.
Mann, M.E., Lees, J.M., 1996. Robust estimation of background noise and signal detection in climatic time series. Clim. Chang. 33, 409–445.
Mantua, N.J., Hare, S.R., Zhang, Y., Wallace, J.M., Francis, R.C., 1997. A Pacific interdecadal oscillation with impacts on salmon production. Bull. Am. Meteorol. Soc. 78, 1069–1079.
Mariotti, A., Zeng, N., Lau, K.-M., 2002. Euro-Mediterranean rainfall and ENSO – a seasonally varying relationship. Geophys. Res. Lett. 29 (12), 59-1–59-4.
Marshall, J., Kushnir, Y., Battisti, D., Chang, P., Czaja, A., Dickson, R., Hurrell, J., McCartney, M., Saravanan, R., Visbeck, M., 2001. North Atlantic climate variability: phenomena, impacts and mechanisms. Int. J. Climatol. 21, 1863–1898.
Mastrangelo, D., Horvath, K., Riccio, A., Miglietta, M.M., 2011. Mechanisms for convection development in a long-lasting heavy precipitation event over southeastern Italy. Atmos. Res. 100, 586–602.
Mestre, O., Domonos, P., Picard, F., Auer, I., Robin, S., Lebarbier, E., Bohm, R., Aguilar, E., Guijarro, J., Vertachnik, G., Klancar, M., Dubuisson, B., Stepanek, P., 2013. HOMER: a homogenization software – methods and applications. Időjárás Quart. J. Hungarian Meteorol. Ser. 117, 47–67.
Meteorological Office, 1962. Weather in the Mediterranean I.General Meteorology, 2nd edition. MO 391b, HMSO, London (362 pp).
Miglietta, M.M., Regano, 2008. An observational and numerical study of flash-flood event over south-eastern Italy. Nat. Hazards Earth Syst. Sci. 8, 1417–1430.
Mohanakumar, K., 2008. Stratospheric influence on tropospheric weather and climate. In: Stratosphere Troposphere Interactions. Springer, pp. 357–399.
Mokhov, I.I., Smirnov, D.A., 2006. El Niño-Southern Oscillation drives North Atlantic Oscillation as revealed with nonlinear techniques from climatic indices. Geophys. Res. Lett. 33, L033708.
Moscatello, A., Miglietta, M.M., Rotunno, R., 2008. Observational analysis of a Mediterranean 'hurricane' over south-eastern Italy. R. Meteorol. Soc. 63 (10), 308–311.
Nicolis, C., 1993. Long-term climatic transitions and stochastic resonance. J. Stat. Phys. 70, 3–14.
Nissen, K.M., Leckebusch, G.C., Pinto, J.G., Renggli, D., Ulbrich, S., Ulbrich, U., 2010. Cyclones causing wind storms in the Mediterranean: characteristics, trends and links to large-scale patterns. Nat. Hazards Earth Syst. Sci. 10, 1379–1391.
Norrant, C., Douguédroit, A., 2005. Monthly and daily precipitation trends in the Mediterranean (1950–2000). Theor. Appl. Climatol. 83, 89–106.
OrtizBevia, M., Perez-Gonzales, I., Alvarez-Garcia, F., Gershunov, A., 2010. Nonlinear estimation of El Niño impact on the North Atlantic winter. J. Geophys. Res. 115 (D21123), 1–10. http://dx.doi.org/10.1029/2009JD013387.
Osipov, G.V., Hu, B., Zhou, C., Ivanchenko, M.V., Kurths, J., 2003. Three types of transitions to phase synchronization in coupled chaotic oscillators. Phys. Rev. Lett. 91, 024101. http://dx.doi.org/10.1103/PhysRevLett. 91.024101.
Paluš, M., Novotná, D., 2004. Enhanced Monte Carlo singular system analysis and detection of period 7.8 years oscillatory modes in the monthly NAO index and temperature records. Nonlinear Process. Geophys. 11, 721–729.
Pasarić, Z., Belušić, D., Klaić, Z.B., 2007. Orographic influences on the Adriatic sirocco wind. Ann. Geophys. 25, 1263–1267.
Pettitt, A.N., 1979. A non-parametric approach to the change-point detection. Appl. Stat. 28, 126–135.
Picard, F., Lebarbier, E., Hoebeke, M., Rigaill, G., Thiam, B., Robin, S., 2011. Joint segmentation, calling and normalization of multiple CGH profiles. Biostatistics 12, 413–428.
Pigot, T.D., 2001. A review of methods of missing data. Educ. Res. Eval. 7 (4), 353–383.
Pikovsky, A., Rosenblum, M., Kurths, J., 2003. Synchronization. A Universal Concept in Nonlinear Sciences, Vol. 12. Cambridge University Press, Cambridge, England.
Polonskii, A.B., Basharin, D.V., Voskresenskaya, E.N., Worley, S., 2004. North Atlantic Oscillation: description, mechanisms, and influence on the Eurasian climate. Phys. Oceanogr. 14, 96–113.
Power, S., Casey, T., Folland, C.K., Colman, A., Mehta, V., 1999. Inter-decadal modulation of the impact of ENSO on Australia. Clim. Dyn. 15, 319–323.
Pozo-Vázquez, D., Esteban-Parra, M.J., Rodrigo, F.S., Castro-Diez, Y., 2001. The association between ENSO and winter atmospheric circulation and temperature in the North Atlantic region. J. Clim. 14, 3408–3420.
Quiroga, R.Q., Kraskov, A., Kreuz, T., Grassberger, P., 2002. Performance of different synchronization measures in real data: a case study on electroencephalographic signals. Phys. Rev. E 65 (4), 041903.
Rimbu, N., Lohmann, G., Felis, T., Pätzold, J., 2003. Shift in ENSO teleconnections recorded by a northern Red Sea coral. J. Clim. 16, 1414–1422.
Rodó, X., Baert, E., Comin, F.A., 1997. Variations in seasonal rainfall in Southern Europe during the present century: relationships with the North Atlantic Oscillation and the El Niño-Southern Oscillation. Clim. Dyn. 13, 275–284.
Romanou, A., Tselioudis, G., Zerefos, G., Clayson, C.-A., Curray, J.A., Andersson, A., 2010. Evaporation – precipitation variability over the Mediterranean and the Black Seas from satellite and reanalysis estimates. J. Clim. 23, 5268–5287.
Rosenblum, M.G., Pikovsky, A.S., Kurths, J., 1996. Phase synchronization of chaotic oscillators. Phys. Rev. Lett. 76, 1804–1807.
Rosenblum, M.G., Pikovsky, A., Kurths, J., Schäfer, C., Tass, P.A., 2001. Phase synchronization: from theory to data analysis. Handb. Biol. Phys. 4 (279–321), 93–94.
Salinger, M.J., Renwick, J.A., Mullan, A.B., 2001. Interdecadal Pacific Oscillation and South Pacific climate. Int. J. Climatol. 21, 1705–1721.
Schafer, J.L., 1997. Analysis of Incomplete Multivariate Data. Chapman and Hall, New York.
Schicker, I., Radanovics, S., Seibert, P., 2010. Origin and transport of Mediterranean moisture and air. Atmos. Chem. Phys. 10, 5089–5105.
Schneider, T., 2001. Analysis of incomplete climate data: estimation of mean values and covariance matrices and imputation of missing values. J. Clim. 14, 853–871.
Sindosi, O.A., Bartzokas, A., Kotroni, V., Lagouvardos, K., 2015. Influence of orography on precipitation amount and distribution in NW Greece: a case study. Atmos. Res. 152, 105–122.
Solomon, S., Qin, D., Manning, M., Chen, Z., Marquis, M., Averyt, K.B., Tignor, M., Miller, H.L., 2007. Technical summary. In: Climate Change 2007: The Physical Science Basis. Contribution of Working Group I to the Fourth Assessment Report of the Intergovernmental Panel on Climate Change. Cambridge University Press.

Staudt, M., Esteban-Parra, M.J., Castro-Diez, Y., 2007. Homogenization of long-term monthly Spanish temperature data. Int. J. Climatol. 27, 1809–1823.
Torrence, C., Compo, G.P., 1998. A practical guide to wavelet analysis. Bull. Am. Meteorol. Soc. 79, 61–78.
Torrence, C., Webster, P.J., 1999. Interdecadal changes in the ENSO-Monsoon system. J. Clim. 12, 2679–2690.
Trenberth, K.E., Jones, P.D., Ambenje, P., Bojariu, R., Easterling, D., Klein Tank, A., Parker, D., Rahimzadeh, F., Renwick, J.A., Rusticucci, M., Soden, B., Zhai, P., 2007. Observations: surface and atmospheric climate change. In: Solomon, S., Qin, D., Manning, M., Chen, Z., Marquis, M., Averyt, K.B., Tignor, M., Miller, H.L. (Eds.), Climate Change 2007: The Physical Science Basis. Contribution of Working Group I to the Fourth Assessment Report of the Intergovernmental Panel on Climate Change. Cambridge University Press.
Tsonis, A.A., Swanson, K., Kravtsov, S., 2007. A new dynamical mechanism for major climate shifts. Geophys. Res. Lett. 34, L13705.
Tulloch, R., Marshall, J., 2012. Exploring mechanisms of variability and predictability of Atlantic meridional overturning circulation in two coupled climate models. J. Clim. 25 (12), 4067–4080.
Ulbrich, U., Lionello, P., Belušić, D., Jacobeit, J., Knippertz, P., Kuglitsch, F.G., Leckebusch, G.C., Luterbacher, J., Maugeri, M., Maheras, P., Nissen, K.M., Pavan, V., Pinto, J.G., Saaroni, H., Seubert, S., Toreti, A., Xoplaki, E., Ziv, B., 2012. Climate of the Mediterranean: synoptic patterns, temperature, precipitation, winds, and their extremes. In: Lionello, P. (Ed.), The Climate of the Mediterranean Region - From the Past to the Future. Elsevier, pp. 301–346.
Venema, V.K.C., Mestre, O., Aguilar, E., Auer, I., Guijarro, J.A., Domonkos, P., Vertacnik, G., Szentimrey, T., Stepanek, P., Zahradnicek, P., Viarre, J., Müller-Westermeier, G., Lakatos, M., Williams, C.N., Menne, M.J., Lindau, R., Rasol, D., Rustemeier, E., Kolokythas, K., Marinova, T., Andresen, L., Acquaotta, F., Fratianni, S., Cheval, S., Klancar, M., Brunetti, M., Gruber, C., Prohom Duran, M., Likso, T., Esteban, P., Brandsma, T., 2012. Benchmarking homogenization algorithms for monthly data. Clim. Past 8, 89–115.
Vicente-Serrano, S.M., Beguería, S., López-Moreno, J.I., García-Vera, M.A., Štěpánek, P., 2010. A complete daily precipitation database for northeast Spain: reconstruction, quality control, and homogeneity. Int. J. Climatol. 30, 1146–1163.
Von Neumann, J., 1941. Distribution of the ratio of the mean square successive difference to the variance. Ann. Math. Stat. 12, 367–395.
Wallace, J.M., Gutzler, D.S., 1981. Teleconnections in the geopotential height field during the Northern Hemisphere winter. Mon. Weather Rev. 109, 784–812.
Walter, K., Graf, H.E., 2002. On the changing nature of the regional connection between the North Atlantic Oscillation and sea surface temperature. J. Geophys. Res. 107 (4338), ACL 7-1–7-13.
Wang, B., 1995. Interdecadal changes in El Niño onset in the last four decades. J. Clim. 8, 267–285.
Wang, G., Kyle, L., Swanson, K.L., Tsonis, A.A., 2009. The pacemaker of major climate shifts. Geophys. Res. Lett. 36, L07708.
Wanner, H., Brönnimann, S., Casty, C., Gyalistras, D., Luterbacher, J., Schmutz, C., Stephenson, D.B., Xoplaki, E., 2001. North Atlantic Oscillation – concepts and studies. Surv. Geophys. 22, 321–382.
Xoplaki, E., 2002. Climate Variability Over the Mediterranean. University of Bern (Ph.D. Thesis).
Yiou, P., Ghil, M., Jouzel, J., Paillard, D., Vautard, R., 1994. Nonlinear variability of the climatic system, from singular and power spectra of Late Quaternary records. Clim. Dyn. 9, 371–389.
Zanchettin, D., Franks, S.W., Traverso, P., Tomasino, M., 2008. On ENSO impacts on European wintertime rainfalls and their modulation by the NAO and the Pacific multi-decadal variability described through the PDO index. Int. J. Climatol. 28, 995–1006.
Zheng, B., Gu, D., Lin, A., Li, C., 2008. Spatial patterns of Tropospheric Biennial Oscillation and its numerical simulation. Adv. Atmos. Sci. 28, 815–823.
Zveryaev, I.I., Hannachi, A.A., 2011. Interannual variability of Mediterranean evaporation and its relation to regional climate. Clim. Dyn. http://dx.doi.org/10.1007/s00382-011-1218-7.